Structural Change and Its Assessment by Fluorescence Spectroscopy in Functional Polymers

YING, JIA
2014

Abstract

The present thesis primarily describes structural changes in polyurethane (PU) shape memory polymer (SMP) and results of experimental studies using fluorescence spectroscopy to detect structural changes in SMP. An easy-to-implement approach to tailoring the shape recovery ratio by annealing is demonstrated. Using PU shape memory polymer, we also developed a sensitive method for detecting tertiary structural changes in polymers, by fluorescence spectroscopy using laser confocal scanning microscopy, which can potentially be utilized as a non-destructive testing method to detect structural changes causing mechanical functional changes such as damage in polymers and polymer composites. The effect of structural changes on mechanical properties in a polymer-based composite system with mechanical function was also investigated on a ternary biodegradable carbon fiber (CF) reinforced hydroxyapatite (HA) / polylactide (PLA) composite. The main body of the thesis consists of five chapters as detailed below.

Chapter 1 introduces background knowledge of polymer degradation, shape memory polymers and their working mechanisms, as well as methods for characterizing properties in polymers.

Chapter 2 studies degradation of a novel biodegradable CF/HA/PLA composite, in order to investigate the structural changes on mechanical properties in functional polymer composites. This material was designed for bone fixation. CF provides strength, while HA provides bioactivity and PLA meets the requirement of degradation. In a three-month in vitro experiment, we measured flexural strength, mass loss, and fracture-surface morphology in certain time intervals. We found that, with increasing degradation time, gaps appeared in the interface between CF and HA/PLA because of PLA hydrolyses. This resulted in mass loss. Flexural strength decreases with increasing degradation time.

Chapter 3 focuses on the relationship between shape memory effect and annealing at a specific temperature for PU SMP from tertiary structural changes point of view. The tertiary structure in polymer means the three-dimensional shaping or folding of the polymer chains. This research is useful to increase the shape recovery ratio of SMP with poor recovery behavior and to manufacture polymers in complex shape from simple-shape molds. At 65°C, we confirmed that the PU SMP film's length change ratio due to annealing is actually the same as the change due to shape memory effect. We also confirmed that we could control the shape recovery ratio by controlling annealing time because annealing and shape memory effect have the same mechanism, which is the change of state from low conformational-entropy states to the recovery of a stable high-entropy state in the polymer. Results for annealing and shape recovery at higher temperatures are left for further confirmation.

Chapter 4 developed a method to detect structural changes in PU SMP by measuring fluorescence intensity from fluorescent dye immersed in this material using laser confocal scanning microscopy. Assuming that the decrease in the length change ratio is attributed to the structural change in polymer, we compared the fluorescence intensity of immersed fluorescent dyes in the shape memory polyurethane samples with that of different thermomechanical cycles. Two fluorescent probes (pyranine and uranine) were used. Experiment results indicate the difference in the fluorescence intensity distribution between the samples with the different length change ratios. This method is sufficiently sensitive to detect the structural changes between samples with the different length change ratios.

Chapter 5 presents the major conclusions and future works of this study. Future works include experiments on controlling complex shape of SMP after thermomechanical cycles, and optimization of the fluorescence spectroscopy by choosing a more suitable fluorescent probe or changing measurement parameters.

Acknowledgements

The writing of this thesis has been one of the most significant academic challenges I have ever had to face. Without the patience, support and guidance of the following people, this thesis would not have been completed. It is to them that I owe my highest gratitude.

First of all I would like to express my heartfelt appreciation to my supervisor Professor Masaki Hojo of the Department of Mechanical Engineering and Science, Kyoto University, for providing me the opportunity to study as his doctoral course student at Mechanics of Adaptive Materials and Structures Lab and guiding me through the whole three years of my study at Kyoto University.

My heartfelt gratitude and appreciation goes to my mentor Associate Professor Masaaki Nishikawa of the Department of Mechanical Engineering and Science, Kyoto University, for his patient guidance and supervision from research topics, experiments, to the discussions about data and paper writing. He is an enjoyable person to be with and one of the smartest people I know. Without him, this thesis could not have been a reality. His guidance has made my study here a thoughtful and fruitful journey.

I also would like to thank Professor Takayuki Kitamura of the Department of Mechanical Engineering and Science, Kyoto University, and Professor Shiro Biwa of the Department of Aeronautics and Astronautics, Kyoto University, for their encouragement, helpful advices and insightful suggestions on improving the quality of this thesis.

Associate Professors Lie Shen and Mao Peng of the Department of Polymer Science and Engineering, Zhejiang University, China, lead me to start researches on polymer science and engineering as an undergraduate student. Their education was one of the reasons to pursue a Ph.D. degree. I will forever be thankful to them. My experience as a master student in Chalmers University of Technology, Sweden, under the supervision of Professor Rodney Rychwalski of the Department of Materials and Manufacturing Technology, helped me to have a better understanding of polymer physics and material engineering. I owe my sincere gratitude to him.

My special thanks to Dr. Yasushi Nakata and Ms. Ikuko Hamagami of Horiba, Inc. for

generously providing trial of their instruments and sharing valuable knowledge on fluorescence measurement. Many thanks to Mr. Hideki Takahashi, Mr. Yoshiyuki Inoue and Mr. Masaaki Sakakura of Nanotechnology Center, Kyoto University, for providing careful guidance of using laser confocal scanning microscopy.

My heartfelt gratitude goes to all the present and graduated students of the past two years at the Adaptive Materials and Structures Lab, Kyoto University. I would like to thank them for always making me feel at home, and more so, for their constant help and support throughout my study period. Special thanks to PhD candidate Manato Kanesaki, for his constant encouragement and discussions about my work and also his great help on my presentation for thesis defense and thesis writing. I would also like to thank Ms. Kiriko Yamaguchi for helping with administrative works during my study here.

I would like to acknowledge the Ministry of Education, Culture, Sports, Science and Technology for the International Doctoral Program in Engineering at Graduate School of Engineering, Kyoto University.

Last, but far from least, my very sincere thanks go to my parents and brother for their patience, unconditional love and support all the time.

Kyoto, August 2014 Ying, Jia

Table of Contents

Chapter 1
Introduction

1. Introduction

Polymer and polymer composites have become indispensable ingredients of human life. Over the last 50 years, the polymer and composite industries are growing rapidly [1]. During the whole lifespan of polymer and polymer composite products, some need good degradation property while some others need stability. For products which have short in service time, good degradability can reduce the influence of plastic wastes to environment [2, 3]. This has offered scientists a possible solution to waste-disposal problems associated with traditional plastics [4]. Therefore, degradability is demanded in packaging industry, paper coating, etc. [5]. Another field which has demand in degradability is biomaterials. Typical applications and research areas are tissue replacement, tissue augmentation, tissue support, and drug delivery [6]. In a lot of cases, the presence of a device/ biomaterial is only temporary needed, so biodegradable materials are better alternatives than biostable ones [6].

Meanwhile, for some polymer and polymer composites which have long lifespan, good stability is needed. For example, thermal stability is needed for polymers which are used outdoors in high temperature [7]. Moreover, for functional polymers, it is important to be aware of the change of functional performance with the time in service. Therefore, the control of materials' stability and understanding the degrees of degradations are of interest.

In this thesis, we first introduced the preparation of a ternary biodegradable carbon fiber (CF) reinforced hydroxyapatite (HA) / polylactide (PLA) composite, and the measurement of degradation in different time intervals in vitro. Second phase of the study was focused on functional polymer: polyurethane (PU) shape memory polymers (SMPs). We studied the relationship of annealing and shape memory effect of this PU SMP, and explained the phenomenon from molecular structural change's point of view, meanwhile proposed a method of controlling shape memory effect by annealing. In the last part, a method which detects structural

change in PU shape memory polymer by fluorescence spectroscopy with the use of laser scanning confocal microscopy was introduced.

1.1 Degradation of polymer and polymer composites

1.1.1 Types of polymer degradation

There are two main types of plastics degradation being researched at present: physical and chemical, and both are closely inter-connected [8]. Chemical degradation involves bond scissions and subsequent chemical transformations [9]. It has been classified as photo-oxidative degradation, thermal degradation, ozone-induced degradation, mechanochemical degradation, catalytic degradation and biodegradation [10]. Physical degradation is the changes in polymer properties with time without involving the bond scission. Normally it relates to the change of polymer conformation from a non- equilibrium state to a relatively equilibrium state by Brownian motion [11], for example, functional fatigue in some functional polymers, etc. Physical degradation is a kind of thermodynamically reversible process. If physically degraded polymer material is heated above melting temperature and quickly cooled down, the property will be recovered to the state before degradation [11].

Degradation reflects changes in material properties such as mechanical, optical or electrical characteristics in crazing, cracking, erosion, and phase separation [5]. Three kinds of main polymer degradation are introduced here:

1.1.1.1 Photo-oxidative degradation

Photo-oxidative degradation is the process of decomposition of the material by light, which is considered as one of the primary sources of damage exerted upon polymeric substrates in environment. The process of photo-oxidative degradation is as follows: the absorption of UV light that has sufficient energy to break the chemical bonds leads to the formation of radical group. After that, propagating reactions of auto-oxidation cycle takes place. It terminated by ‘mopping up’ the free radicals to create inert products.

Methods for photo-degradation are natural weathering method and artificial weathering method. In natural method, outdoor exposure is performed on samples, with temperature and humidity of

the location [5]. While artificial method is in laboratory using environmental chambers and artificial light sources to replicate outdoor conditions. The advantage of using artificial method is that it can quickly assess the degradability of material but disadvantage is, the quicker the test the lower is the correlation to real behavior [12].

1.1.1.2 Thermal degradation

Normally, photo chemistry and thermal degradations are similar. Both are classified as oxidative degradation. The main difference between the two is the sequence of initiation steps leading to auto-oxidation cycle. The thermal degradation of polymers consists of two distinct reactions, which occur simultaneously. One is a random scission of links, causing a molecular weight reduction, and the other is a chain-end scission of C-C bonds, generating volatile products [13].
Methods for thermal degradation are batch reactor method and thermogravimetric analysis (TGA). Batch reactor is a glass reactor which allows temperature increasing to degradation temperature under nitrogen protection. The gaseous products can be condensed to liquid products and measured. The solid residue can be identified by FTIR spectrometer for composition analysis [14]. TGA method is for the investigation of oxidative and thermal degradation of the polymers by weighing initial weight, actual weight at each point and final weight [15].

1.1.1.3 Biodegradation

Biodegradation is defined as the propensity of a material to get breakdown into its constituent molecules by natural processes. It has several different mechanisms, depends on the properties of materials. For example, for polymers which have good hydrophilicity, hydration results from disruption of secondary and tertiary structure stabilized by van der Waals forces and hydrogen bonds. During and after hydration, the polymer chains may become water soluble, backbone of polymer may be cleaved because of hydrolysis, which results in the loss of polymer strength. [16].
When choosing a test method for biodegradation, most important factor is selecting the test procedure based on the nature of plastic and the conditions of study environment. Soil burial method is very frequently used for the determination of biodegradability of plastic in natural

environment. Phosphate buffered saline (PBS) is a buffer solution commonly used in biological research which has osmolarity and ion concentration similar to human body [17]. It is often chosen in biodegradation study when vitro simulation is needed.

1.1.2 Types of polymer composite degradation

Polymer composites have two phases, which are polymer matrix phase and reinforcing phase such as fibers, sheets or particles [18]. Normally, reinforcing phase contributes most to the material strength. Matrix serves to transfer applied structured loads to the fibers as well as binding the fibers together and protecting them from environment. Interface between these two phases governs these load transfer characteristics and contributes to the overall damage tolerance of the structure [19, 20].

Since matrix part is polymer, all the mechanisms that cause neat polymer degradation as introduced in last section could cause degradation in polymer composites. Therefore, in this section, degradation mechanisms which influence matrix – reinforcing interface are introduced.

1.1.2.1 Degradation due to moisture exposure

Moisture penetration into composite materials is conducted by diffusion. Some mechanisms involve direct diffusion of water molecules into the matrix and in some cases into the fibers. Some other mechanisms indicate capillary flow of water along the fiber/matrix interface, followed by diffusion from the interface into the bulk resin, and transport by microcracks [21]. Moisture diffuses into matrix, which leads to dilatation and also chemical changes, such as plasticization and hydrolysis [22]. The first effect of water to be discussed here is hygroelasticity and swelling. Hygroelasticity is the dimensional response of the material to water penetration. It is resulting from the build-up of internal stresses due to accumulation of water molecules within the polymer network and at the interface. This in long-term would result in failure of the matrix and of the interface. Also failure could be caused from two other contributions. One is hydrolysis, in case hydrophilic groups exist [23]. The other is plasticization of polymeric matrix. Water acts as an internal lubricant, decreasing the energy barriers for chain segment movement. Moreover, water can break hydrogen bonds which present in the polymer and act similar to cross-links in raising glass transition temperature (Tg) [24]. Only a percent or so of water is

sufficient to yield large Tg reductions. A direct consequence is that, under some given conditions, the composite structure might operate at a temperature which is higher than actual Tg, thus failure happens.

1.1.2.2 Degradation due to temperature effects

Various applications of composite materials expose to environment whose temperature can vary over a wide range. The temperature effect derives from mechanical stresses can be induced in composites containing constituents with different thermal expansivities [25, 26]. For example, epoxy resin has a linear coefficient of thermal expansion of about 60×10^{-6} $°C^{-1}$, while that of Kevlar aramid fiber is about -6×10^{-6} $°C^{-1}$ [27] For composites which already have residual stresses in the structure, the stress magnitude can be changed due to environment temperature changes. During temperature changes, tensile constraint in matrix may lead to thermal cracking, which in turn, facilitates moisture penetration into the structure.

1.1.3 Degradable chemical compounds - PLA

Poly vinyl alcohol (PVA), polyesters, polyethylene and polymer blends such as starch/polyethylene, starch/polyester are common degradable polymers [28]. Polyesters play a predominant role as degradable polymers due to their potentially hydrolysable ester bonds [29]. Among these, poly (lactic acid) (PLA), which belongs to the family of aliphatic polyesters, is one of the most widely used synthetic degradable polymers due to its many favorable properties such as availability, relatively good strength, biocompatibility, etc. [30, 31, 32].

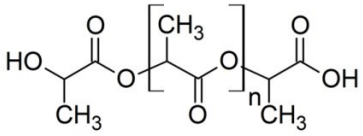

Fig.1.1 A sketch of chemical structure of PLA

PLA degradation is dependent on many factors such as molecular weight, crystallinity, purity, temperature, pH, presence of terminal carboxyl or hydroxyl; groups, water permeability, and additives acting catalytically that may include enzymes, bacteria or inorganic fillers [33]. Pyrolysis is chemical decomposition of a condensed substance by heating. For waste

degradation, it provides a method to dispose and convert PLA waste origins into higher value fuel [34]. PLA can also be hydrolyzed and recycled back to the monomer [35]. Moreover, reports show PLA can be decomposed into carbon dioxide and water in a "controlled composting environment" in fewer than 90 days [36]. Also, it has been confirmed that PLA is naturally degraded in soil or compost. The products of the PLA hydrolytic degradation can be totally assimilated by microorganisms such as bacteria or fungi [37, 38, 39].

Because degradation properties mentioned above, PLA is a commodity resin for general packaging applications. In the form of fibers and non-woven textiles, PLA can be used as upholstery, disposable garments, awnings, feminine hygiene products, and nappies. Since PLA is biodegradable, it has extensive applications in biomedical fields, including suture, bone fixation material, drug delivery microsphere, and tissue engineering [40, 41].

1.2 Polyurethane Shape Memory Polymers

1.2.1 Shape memory thermomechanical cycle and working mechanisms

Shape memory polymers (SMPs) are polymers with the ability to store and recover strains on the order of several hundred percent when subjected to a particular thermomechanical cycles [42]. They have been widely researched since the 1980s and are an example of a promising smart material [43, 44, 45].

A shape memory cycle represents its response when subjected to a thermomechanical cycle that allows for deforming and fixing of a temporary shape and recovering the permanent shape [46]. For simplicity, the thermal cycle here is described in tensile deformation of a thermally activated SMPs. Four successive steps are needed for a thermal cycle:

1. Deformation: The sample is deformed to a predetermined strain at the temperature T_d above transition temperature (T_{trans}), which is glass transition temperature (T_g) for amorphous polymers and melting point (T_m) for crystalline polymers.
2. Cooling: Under the imposed deformation constraint, the sample is cooled to a setting temperature. Normally faster cooling prevents excessive stress or strain relaxation, if any.
3. Fixing: The initial deformation constraint is released after cooled down.

4. Recovery: The temporarily deformed sample is heated back to above T_{trans}.

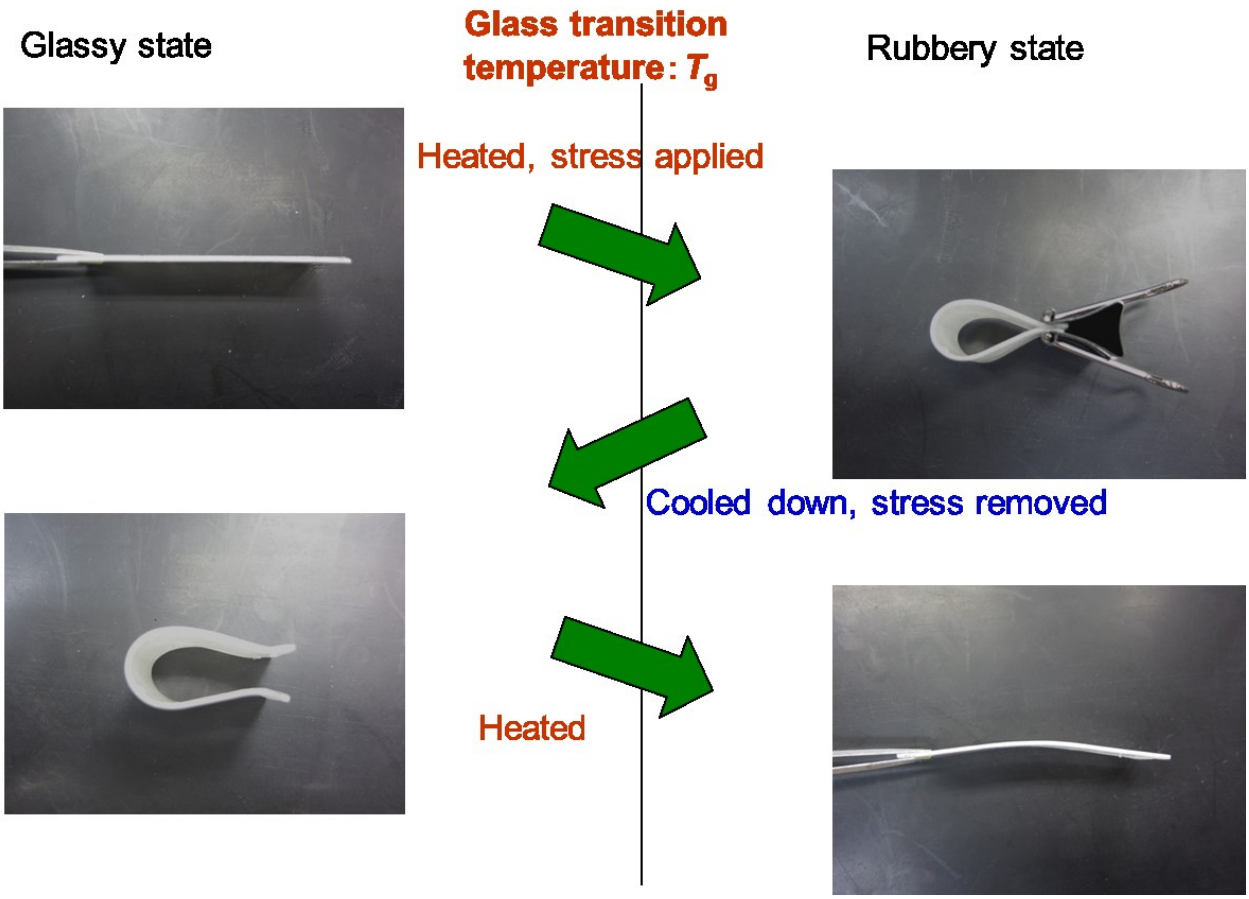

Fig.1.2 Schematic of shape memory effect during a typical thermomechanical cycle. Picture by Y. Sekiya.

Huang [47] proposed three major possible working mechanisms for shape memory effect in polymers. Heating responsive polymer was used as an example here:

1. Heat SMP to above its glass transition temperature (Tg) and deform it easily (since it is in the rubbery state). After cooling back to below its Tg, followed by unloading to remove the constraint, the distorted shape is largely maintained, apart from some elastic recovery (since the polymer is in the glassy state). Heating again to above its Tg, micro-Brownian motion enables the polymer to return to the original shape. Poly(methyl methacrylate) (PMMA) is a typical example of a polymer this mechanism applies to.

2. In the second working mechanism, there are two segments/domains in a polymer, netpoints and molecular switches. The netpoints, which are connected by chain segments, determine the permanent shape of SMP. They can be chemical (covalent bonds) or physical (intermolecular interactions) nature. Molecular switches are sensitive to external stimulus. Polyurethane, which has a typical hard/soft-segment structure, is a good example. Scheme about this mechanism is shown in the figure below.

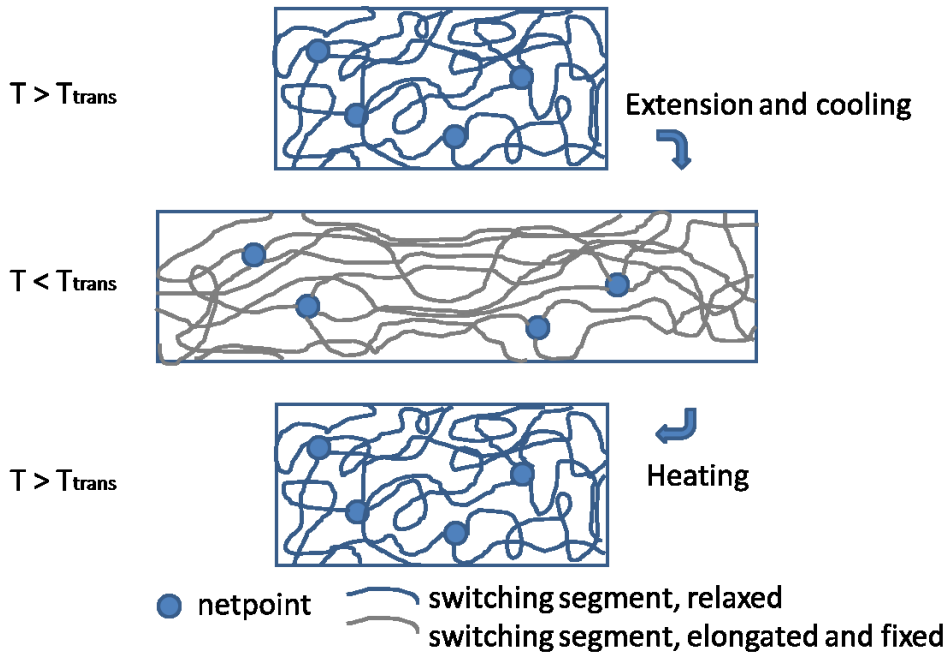

Fig.1.3 Molecular mechanism of netpoints and molecular switches. T_{trans} is the thermal transition temperature of the switching phase. Adapted from [48].

3. The third mechanism utilizes the polymer itself as both the elastic and transition component. Here we take wax as an example. When wax is heated to achieve partial melting, the solid part acts as the elastic component, while the melted part functions essentially as the transition component.

1.2.2. Application and different opinions on SMPs

A lot of articles have reported different applications of SMP materials, ranging from outer space to biomaterials. Especially for deployable components and structures in aerospace, they are being more and more developed and researched recently. Hinges, trusses, booms, antennas, optical reflectors, morphine skins are some examples [43, 49, 50, 51]. A review article by Ratra and Karger-kocsis [52] covers recent research on SMPs which have potential applications as sensors and /or actuators. Moreover, many researches are focusing on the use of SMPs in biomedicine area. Lendlein and his co-workers [53] did research on photo-responsive degradable SMPs for medical applications. One of the large groups in SMP family is polyurethane SMP, the excellent biocompatibility allows it becoming one of the candidate materials for clinical devices when contacted or implanted in the human body [54, 55]. Wache et al. [56] have conducted a feasibility study on the development of a polymer vascular stent with an SMP as drug delivery system.

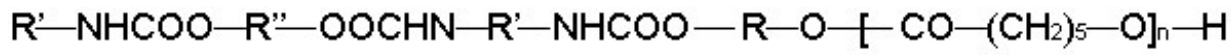

Fig.1.4 A polyurethane SMP structure. Left part is diisocyanate as hard segment, polyol part acts as soft segment. Here polyol is 1,6-hexanediol. Modified from [57].

Though SMPs are receiving more and more attentions in the recent 20 years, possible applications using SMPs are in various areas, some researchers consider shape memory effect is a kind of intrinsic property of normal polymer materials since shape memory is based on viscoelasticity which is intrinsic property to polymers [58, 59, 60]. Meanwhile some researchers stated opposite [44, 61, 62]. According to Rousseau [46], adequate material and structural design is necessary for polymeric systems to exhibit shape memory behavior, which is to restore the

temporarily fixed residual inelastic deformation once reheated to the rubbery state. In contrast, ordinary polymers do not at all, or only to a low extent, recover from such residual inelastic deformation.

In Ratna and co-worker's review [52], they also supported the view that shape memory effect is not intrinsic property and a figure on the difference of dynamic modulus versus temperature between ordinary crosslinked polymer and SMP was shown as below:

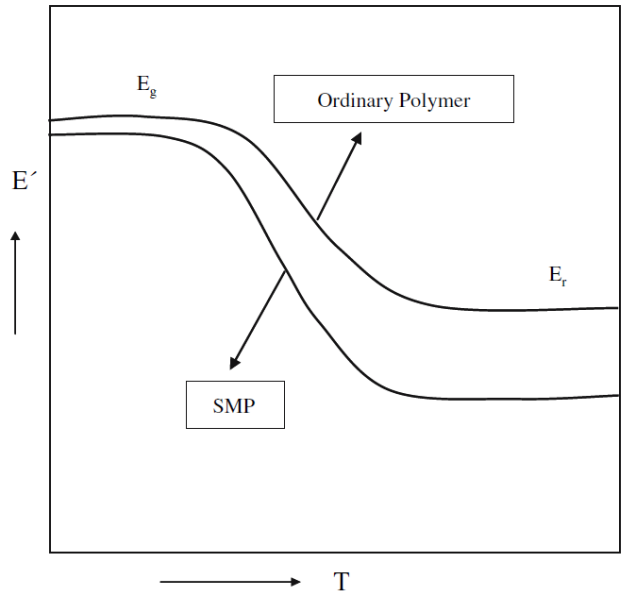

Fig.1.5 Typical dynamic modulus versus temperature plots of an ordinary crosslinked polymer and SMP [52]. E' is dynamic modulus, which means ratio of stress to strain under vibratory conditions.

A high elasticity ratio Eg/Er (Eg: glassy modulus, Er: rubbery modulus) allows for an easy shaping at T > Ts (shape memory temperature) and a great resistance to the deformation at T < Ts. Thus only polymers meet the above criteria are qualified for shape memory applications.

1.3 Assessments for studying polymers and fluorescence spectroscopy

1.3.1 Methods for characterizing and analyzing polymers

There are many experimental methods for studying structural information of polymers. For example, Infrared (IR) and Raman spectroscopy, which base on polymer materials' vibrational properties [63], provide information about chemical structures, conformation, configuration, chain arrangement, etc. [64]; Nuclear magnetic resonance (NMR) and Electron spin resonance (ESR) which use spin resonance, can provide information about chemical composition, average molecular weight and molecular weight distribution [65]. Wide Angle X-Ray Scattering (WAXS) and Small Angle X-Ray Scattering (SAXS) are also common methods for studying polymers based on principles of diffraction. They can be used for measuring crystallinity, size of spherulite, and spinodal decomposition during phase disengagement [64]. Electron microscopy such as Scanning Electron Microscopy (SEM) and Transmission Electron Microscopy (TEM) are also common methods to observe and analyze polymers. TEM provides topographical, morphological, compositional and crystalline information. TEM cannot image through samples thicker than 200nm because electrons cannot readily penetrate sections that thick [66]. SEM is a powerful magnification tool that utilizes focused beams of electrons to obtain information. It can image morphology of samples with high resolution, including bulk material, coatings, sectioned materials, etc. [64]. Thermal analysis provide material characteristics data in relation to temperature and time. They help us to understand polymeric formulations, process history and physical properties of materials. They include Differential Scanning Calorimetry (DSC), Dynamic Mechanical Analysis (DMA), Thermomechanical Analysis (TMA), Thermogravimetric Analysis (TGA), etc. [67].

1.3.2 Laser confocal scanning microscopy and fluorescence spectroscopy

Though as introduced in last section that there are many methods which based on different mechanisms can characterize and analyze polymer materials, they are not enough to deal with all the needs. For example, DSC can measure crystallinity of polymers. Also it can speculate the structural change from the change of crystallinity. However if the structural change is subtle and

no obvious crystallinity change observed, it is difficult to speculate structural change. Another example, SEM and TEM are normally used to obtain images of the morphology of polymers. They also possess some drawbacks. Firstly, the preparation of the samples usually causes problems. Moreover, staining methods have to be applied to get good contrast, which could give risk to artefacts. Furthermore these methods are destructive, i.e. the material has to be broken or cut before the morphology can be examined. Finally, to obtain a three-dimensional picture of the morphology of the polymer materials, many different samples are required for these techniques [68].

Laser Confocal Scanning Microscopy (LCSM) is an important non-destructive method in biology and materials science, due to attributes that are not readily available using other traditional methods [69, 70, 71, 72].

Scan head is the core part of LCSM. It is responsible for rasterizing the excitation scans, as well as collecting the photon signals from the specimen that are required to assemble the final image. A typical scan head contains inputs from the external laser sources, fluorescence filter sets and dichromatic mirrors, a galvanometer-based raster scanning mirror system, variable pinhole apertures for generating the confocal image, and photomultiplier tube detectors tuned for different fluorescence wavelengths [69, 73].

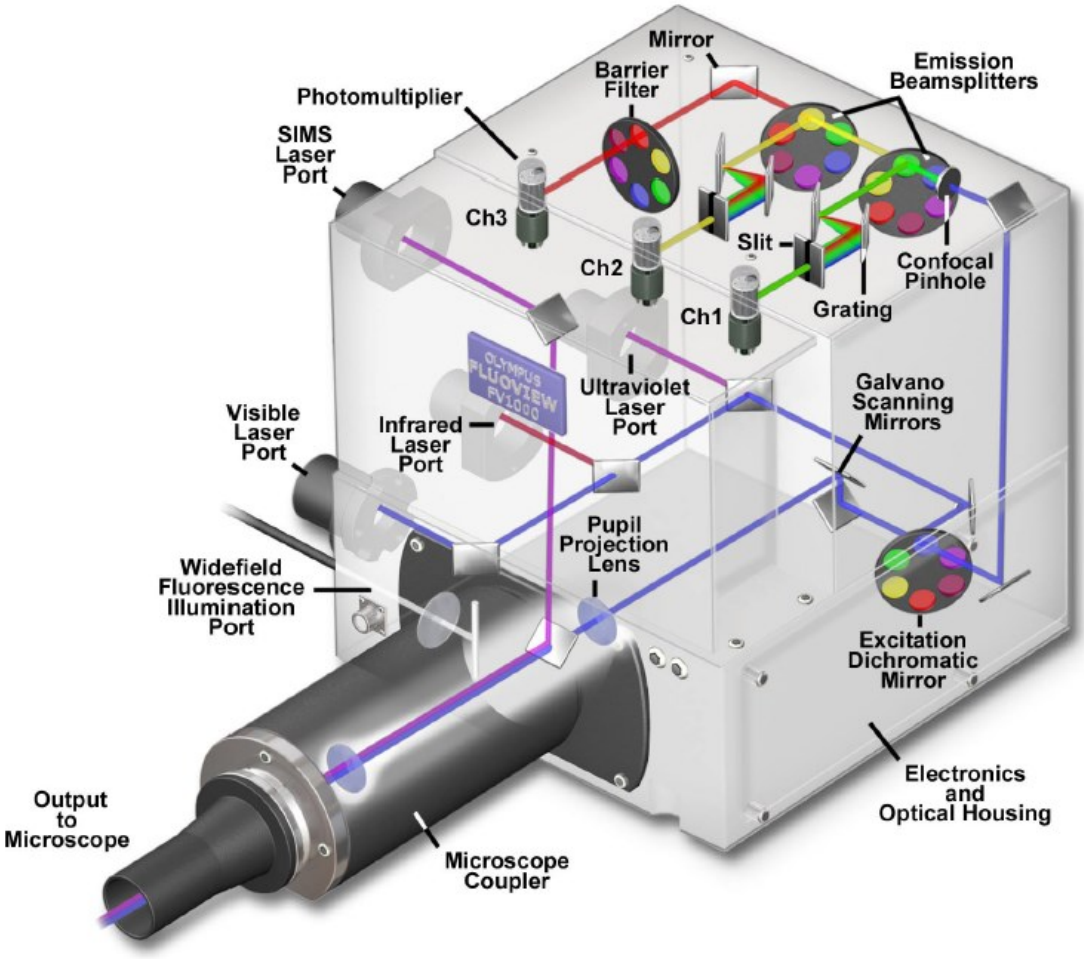

Fig.1.6 A general arrangement of scan head components in LCSM. Picture from NS. Claxton, etc [69].

1.4 Structural changes in polymers

Structural features of polymers are usually described at three levels of complexity: primary structure, secondary structure and tertiary structure [74].

Primary structure refers to the atomic composition and chemical structures of the monomer, which is the building block of the polymer chain. By definition, a polymer is a chain of atoms hooked together by primary valence bonds.

Secondary structure refers to the size and shape of an isolated single molecule. The size can be discussed in terms of molecular weight, and the shape of the polymer molecule is influenced by

conformation, which is the arrangement established by rotation about primary valence bonds.

Tertiary structure is the way how a large number of polymer molecules aggregate. The forces responsible for molecular aggregation are the intermolecular secondary bonding forces. Different arrangements of molecules lead to different tertiary structures. For example, irregular amorphous polymer material, oriented amorphous polymer material and crystalline polymer material have different tertiary structures.

Figure 1.7 demonstrates different structures in primary (a), secondary (b), tertiary (c) level.

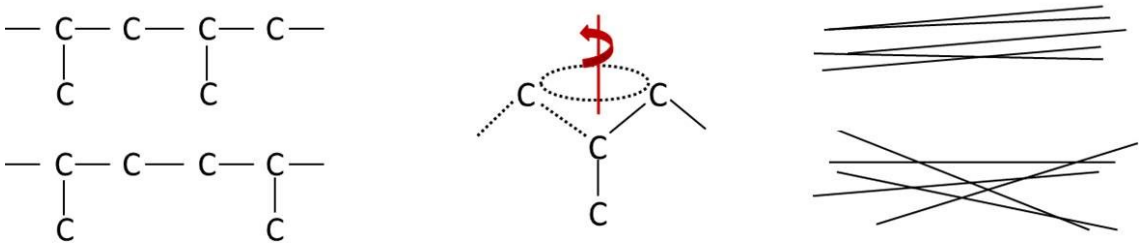

(a) (b) (c)

Fig. 1.7 Different structures in primary (a), secondary (b) and tertiary (c) level.

The chemical and electrical properties of a polymer are directly related to the chemistry of the constituent monomers, which is the primary structure. The physical and mechanical properties of polymers, on the other hand, are largely a consequence of secondary and tertiary structures.

In this thesis, structural change in Chapter 2 is in a secondary level, while Chapter 3 and 4 focus on the tertiary structural change and its assessment.

1.5 Objective of this research

Structural changes affect the performance of polymer products. Subtle changes to polymer structure have a great influence on the chemical and physical, mechanical properties of a polymer material. Thus it is important to understand how structure changes in polymer materials and develop methods to detect these changes.

Specifically, when it comes to shape memory polymers (SMPs), a thorough understanding of how shape recovery takes place is necessary in order to design or modify their properties. Recovery ratio is an important factor when characterizing SMPs' structural performance. In some

SMPs, a recovery ratio close to 100% can be achieved. However, not all the SMPs have such a good recovery ratio. Some researches are also studying shape recovery ratio of certain bio-SMP materials [75, 76, 77]. Therefore, there is much to be gained by looking closer into this subject and finding ways to control recovery ratios more effectively.

In the present study, we were interested in developing a suitable experiment method to detect tertiary structural changes in SMPs at different thermomechanical cycles. While currently there are many experiment methods for characterizing polymers' structures (as introduced in section 1.3.1), none of them can easily detect differences between different modes of polymer chain aggregation. The method used in this study, however, is expected better able to detect damage in polymers and polymer composites as a non-destructive testing method.

Our objectives are:

1) To gain a thorough understanding of effect of structural change on mechanical properties during degradation by measuring degradation properties in the new CF/HA/PLA material for bone fixation that we designed.
2) To identify the principle of shape memory effect from polymer structural point of view and to propose a new method for controlling shape recovery ratio by annealing.
3) To develop a new experiment method to detect tertiary structural change by measuring fluorescence spectroscopy at different depths of material by LCSM.

References:

1. M. Ashby, Materials selection in mechanical design, 2nd edition, 1999, Cambridge University Press.

2. A. Karaduman, Pyrolysis of polystyrene plastic wastes with some organic compounds for enhancing styrene yield. J. Energy sources, 2002, 667.

3. GJL. Griffin, Chemistry and technology of biodegradable polymers. 1994; Springer.

4. AK. Mohanty, Biofibres, biodegradable polymers and biocomposites: An overview. Macromol. Mater. Eng. 2000, 1.

5. B. Singh, Mechanistic implications of plastic degradation. Polymer Degradation and stability. 2008, 561.

6. M. Martina, Biodegradable polymers applied in tissueengineering research: a review. Polym Int. 2007, 145.

7. A. Leszczynska, JAK. Njuguna, K. Pielichowski, JR. Banerjee, Polymer/montmorillonite nanocomposites with improved thermal properties: Part I. Factors influencing thermal stability and mechanisms of thermal stability improvement. Thermochim Acta, 2007, 75.

8. K. Sylvia, Degradation of polymers, Materials World, 1995, 377.

9. J. Pospisil, Z. Horak, Z. Krulis, S. Nespurek, The origin and role of structural inhomogeneities and impurities in material recycling of plastics. Macromol Symp 1998, 247.

10. N. Grassie, G. Scott. Polymer degradation and stabilization. 1985; Cambridge University Press.

11. CZ. Wang, Properties of materials, 1st edition, 2001; Beijing University of Technology Press.

12. ASTM D4674-89, Standard test method for accelerated testing for color stability of plastics exposed to indoor fluorescent lighting and window-filtered daylight. ASTM International, 1989.

13. K. Murata, Y. Hirano, Y. Sakata, MA. Uddin, Basic study on a continuous flow reactor for

thermal degradation of polymers. J Anal App Pyrolysis 2002, 71.

14. T. Bhaskar, T. Matsui, J. Kaneko, MA. Uddin, Muto A, Y. Sakata, Novel calcium based sorbent (Ca-C) for the dehalogenation (Br, Cl) process during halogenated mixed plastic (PP/PE/PS/PVC and HIPS-Br) pyrolysis. Green Chem 2002, 372.

15. LB. Pierella, S. Renzini, D. Cayuela, OA. Anunziata. Catalytic degradation of polystyrene over ZSM-11 modified materials. Second Mercosur cong. on chem. eng., 4th Mercosur cong. on process systems eng; 2005.

16. T. Ishigaki, Y. Kawagoshi, MIM. Fujita. Biodegradable hydrogels for drug delivery. 1993; CRS Press.

17. J. Sambrook, EF. Fritsch, T. Maniatis, Molecular cloning: a laboratory manual, 2nd ed., 1989; Cold Spring Harbor Laboratory Press.

18. R. Rychwalski, Composite and nanocomposite materials, 2nd edition, 2008; Goteborg.

19. MCY. Niu, Composite airframe structures: practical design information and data. 1992; Commilit Press Ltd.

20. BG. Kumar, RP. Singh, T. Nakamura, Degradation of carbon fiber reinforced epoxy composites by ultraviolet radiation and condensation. J. Comp Mater, 2002, 2713.

21. K. Friedrich, editor, Application of fracture mechanics to composite materials, Composite Materials Series 6, 1989; Elsevier.

22. T. Nakamura, RP. Singh, P. Vaddadi, Effects of Environmental Degradation on Flexural Failure Strength of Fiber Reinforced Composites. Experimental Mechanics , 2006, 1.

23. LR. Bao, Moisture absorption and hygrothermal aging in a bismaleimide resin and its carbon fiber composites. Doctor paper, University of Michigan, 2001.

24. HH. Yang, Kevlar Aramid Fiber Z, 1992; John Wiley & Sons.

25. CC. Chamis, NASA report TM-78835, 1978.

26. JL. Camahort, EH. Renhack, WC Coons, ASTM-STP-602 ,1976, 37.

27. S. Rojstaczer, D. Cohn, GJ. Marom, Thermal expansion of Kevlar fibres and composites, Mater. Sci. Lett. 1985, 1233

28. K. Leja, G. Lewandowicz, Polymer Biodegradation and Biodegradable polymers – a review, Polish J. of Environ. Stud. 2010, 255.

29. KM. Nampoothiri, NR. Nair, RP. John, An overview of the recent developments in polylactide (PLA) research. Bioresource Tech. 2010, 8493.

30. V. Piemonte, F. Gironi, Kinetics of Hydrolytic Degradation of PLA, J Polym Environ 2013, 313.

31. LD. Harris, BS. Kim, DJ. Mooney, J. Open pore biodegradable matrices formed with gas foaming, Biomed. Mater. Res.1998, 396.

32. RC. Thomson, AG. Mikos, E. Beahm, LC. Lemon, Satterfield WC, Aufdemorte TB, Miller MJ, Guided tissue fabrication from periosteum using preformed biodegradable polymer scaffolds. Biomaterials 1999, 2007.

33. KI. Park, MA. Xanthos, Study on the degradation of polylactic acid in the presence of phosphonium ionic liquids. Polym. Degrad. Stab. 2009, 834.

34. W. Gang, L. Aimin, Thermal decomposition and kinetics of mixtures of polylactic acid and biomass during copyrolysis. Chin. J. Chem. Eng. 2008, 929.

35. R. Auras, B. Harte, S. Selke, An overview of polylactides as packaging materials. Macromol. Biosci. 2004, 835.

36. VM. Ghorpade, A. Gennadios, MA. Hanna, Laboratory composting of extruded poly (lactic acid) sheets. Bioresour. Technol. 2001, 57.

37. H. Tsuji, A. Mizuno, Y. Ikada, Blends of aliphatic polyesters. III. Biodegradation of solution-cast blends from poly (L-lactide) and poly (ecaprolactone). J. Appl. Polym. Sci 1998, 2259.

38. S. Li, M. Tenon, H. Garreau, C. Braud, M. Vert , Enzymatic degradation of stereocopolymers derived from L-, DL- and meso-lactides. Polym. Degrad. Stab. 2000, 85.

39. A. Hoshino, M. Tsuji, M. Ito, M. Momochi, A. Mizutani, K. Takakuwa, Biodegradable polymers and plastics. In: Chiellini, E., Solaro, R. (Ed.), Study of the Aerobic Biodegradability of Plastics Materials Under Controlled Compost, 2003; Plenum Press.

40. YM. Zhao, ZY. Wang, J. Wang, HZ. Mai, B. Yan B, F. Yang, Direct synthesis of poly (D, L-lactic acid) by melt polycondensation and its applications in drug delivery. J. Appl. Polym. Sci. 2004, 2143.

41. R. Mehta, V. Kumar, H. Bhunia, SN. Upadhyay, Synthesis of poly (lacticacid):a review. J. Macromol. Sci. Polym. Rev. 2005, 325.

42. K. Otsuka, CM. Wayman, Shape memory materials, 1998; Cambridge University Press.

43. JS. Leng, X. Lan, YJ. Liu, SY. Du, Shape-memory polymers and their composites: stimulus methods and applications, Prog. in Mater Sci. 2001, 1077.

44. M. Behl, A. Lendlein, Shape-memory polymers. Mater Today 2007, 20.

45. A. Lendlein, S. Kelch, Shape-memory polymers. Angew Chem Int. 2002, 2034.

46. IA. Rousseau, Challenges of shape memory polymers: a review of the progress toward overcoming SMP's limitations. Polym. Eng. Sci. 2008, 2075.

47. WM. Huang, Shape memory polymers (SMPs) - current research and future applications, 2013, (http://www.azom.com/article.aspx?ArticleID=6038)

48. M. Behl, J. Zotzmann, A. Lendlein, Shape memory polymers and shape changing polymers, Adv Polym Sci, 2010, 1.

49. BK. Kim, Shape memory polymers and their future development. Express Polym Lett. 2008, 614.

50. SC. Arzberger, NA. Munshi, MS. Lake, Elastic memory composites for deployable space structures. (http://www.CTD-materials.com)

51. X. Lan, JS. Leng, Design of a deployable antenna actuated by shape memory alloy hinge. Mater Sci Forum 2007, 1567.

52. D. Ratna, J. Karger-Kocsis, Recent advances in SMP and composites: a review, J Mater Sci 2008, 254.

53. A. Lendlein, H. Jiang, O. Junger, R. Langer, Light-induced shape-memory polymers. Nature 2005, 879.

54. FE. Feninat, G. Laroche, M. Fiset, D. Mantovani, Shape memory materials for biomedical applications. Adv Eng Mater 2002, 91.

55. W. Sokolowski, A. Metcalfe, S. Hayashi, L. Yahia, J. Raymond, Medical applications of shape memory polymers, Biomed Mater 2007, 23.

56. HM. Wache, DJ. Tartakowska, A. Hentrich, MH. Wagner. Development of a polymer stent with shape memory effect as a drug delivery system. J Mater Sci Mater Med 2003, 109.

57. JL. Hu, Shape memory polymers and textiles. In: Characterization of shape memory properties in polymers. 2007; CRC Press.

58. K. Gall, P. Kreiner, D. Turner, M. Hulse, Shape memory polymers for microelectromechanical systems. J Microelectromech Syst 2004, 472.

59. C. Liu, SB. Chun, PT. Mather, L. Zheng, EH. Haley, EB. Coughlin, Chemically Crosslinked Polycyclooctene: Synthesis, Characterization, and Shape Memory Behavior, Macromolecules, 2002, 9868.

60. C. Liu, H. Qin, PT. Mather, Review of progress in shape memory polymers, J. Mater. Chem, 2007, 1543.

61. CP. Buckley, C. Prisacariu, A. Caraculacu, Novel triol-crosslinked polyurethane and their thermorheological characterization as shape-memory materials. Polymer, 2007, 1388.

62. F. Li, Y. Chen, X. Zhang, M. Xu, Shape memory effect of polyethylene nylon 6 graft copolymers. Polymer, 1998, 6929.

63. MP. Stevens, Polymer Chemistry: An Introduction, 3rd Edition, 1999; Oxford University Press.

64. MJ. He, Polymer Physics, 3rd edition, 2008; Fudan University Press.

65. SD. Hantan, Chem. Rev. 2001, 121, 527

66. T. Vogt, W. Dahmen, PG. Binev, Modelling Nanoscale imaging in electron microscopy 2012; Springer.

67. LN. Zhang, Recent analysis methods on polymer physics, 2003; Wuhan University Press.

68. H. Verhoogt. Confocal laser scanning microscopy: a new method for determination of the morphology of polymer blends, Polymer, 1993, 1325.

69. NS. Claxton, TJ. Fellers, MW. Davidson, Encyclopedia of medical devices and instrumentation, 2006; John Wiley & Sons.

70. JB. Pawley, Handbook of biological confocal microscopy, 1995; Plenum Press.

71. PM. Conn, Confocal microscopy in methods in enzymology, 1999; Academic Press.

72. M. Gu, Principles of three-dimensional imaging in confocal microscopes, 1996; World Scientific.

73. L. Mongan, J. Gormally, A. Hubbard, Calcium Signaling Protocols. 2nd Edition, 2006; Springer.

74. RO. Ebewele, Polymer Science and Technology, 2000, CRC Press.

75. K. Gall, CM. Yakacki, Y. Liu, R. Shandas, N. Willett, KS. Anseth, Thermomechanics of the shape memory effect in polymers for biomedical applications, J. Biomed. Mater. Res. A. 2005, 339.

76. CM. Yakacki, R. Shandas, C. Lanning, B. Rech, A. Eckstain, K. Gall, Unconstrained recovery characterization of shape-memory polymer networks for cardiovascular applications, Biomaterials, 2007, 2255.

77. CM. Yakacki, R. Shandas, D.Safranski, AM. Ortega, K. Sassaman, K. Gall, Strong, tailored, biocompatible shape-memory polymer networks, Adv. Funct. mater. 2008, 2428.

Chapter 2

Preparation and degradation properties of CF/HA/PLA biocomposites

2.1 Introduction

The traditional ways for recovering bone defect are autotransplantation or allotransplantation, due to the scarcity of the possible tissues, the man-made biological material has been receiving a great deal of interest. At first, metals such as stainless steel and titanium alloy are taken for the internal fixation of bone fracture. Compare with the natural bone tissue, these materials characterize high modulus of elasticity. However numerous studies have shown that these rigid metal plates interfere with normal bone physiology by stress shielding of the bone beneath the plates [1-5]. Also metals can't degrade *in vivo*. People would suffer the extra pain during the surgery to fetch the fixation material.

Hydroxyapatite (HA) is the main inorganic component of bone with great bioactivity and bone bonding ability [6-8]. Polylactide (PLA) is widely used in the bone fixation material and surgical suture because of its good degradation [9-11]. However, the low mechanical strength of the pure PLA can't meet the requirement of the repairing of weight bearing bones which limits the application.

Nowadays, inorganic/polymer biomaterials have been the subjects of intense study in surgical reconstruction and bone tissue engineering [12-15]. HA/PLA composite becomes an important representative of these materials since they combine the osteoconductivity and bone bonding ability of HA with the absorbability and the easy processing property of the polymer matrix PLA [16-19]. Nevertheless, the mechanical strength still fails to meet the demands of the fixture of weight bearing bones. Carbon fiber (CF) was widely chosen as a reinforced material in the bone implant for its great biocompatibility and high strength. Though the long-term effect of carbon

fiber in the living tissues is still an opening question, many researches indicated that the bone grew on the exposed carbon fibers and cause no inflammation [20-22]. Furthermore, Czajkowska and Bhiewicz reported that, by oxidizing treatment of carbon fibers with nitric acid as mentioned in our paper, the powders of carbon fiber can be phagocytized [23]. CF reinforced HA/PLA composite not only improves the mechanical properties, but also keeps the advantages of HA/PLA composite material. The flexural and shear strength along the fiber direction is believed to be still poor. However, most of the time fibers are perpendicular to the direction of the applied load when the implanted material located in the tensile area of the construction. It is hopefully to be the internal fixation material with its good bioactivity, absorbability, degradation and high mechanical strength.

2.2 Materials and methods

2.2.1 Surface treatment of CF

CF (T300, Toray Industries, Inc. Japan) and HNO_3 were introduced into a flask. The mixture was heated up to 70°C, refluxing and oxidation for 5h. After the treatment, CF was washed with vast amount of deionized water, the resulting CF was dried for 24h before use. The surface areas of CF before and after the oxidation were determined by a gas sorption analyzer (AUTOSORB-1-C, QUANTACHROME Apparatus company, USA).

2.2.2 Preparation of CF/PLA/HA composites

Weighed HA (Sinopharm Chemical Reagent Co. Ltd, China), PLA (M_n＝172000, M_w＝214000, Zhejiang Hisun Biomaterials Co. Ltd, China) in the mass ratio of HA to PLA 2.5/97.5, 5/95, 10/90, 15/85, 20/80, 25/75, 30/70. First, solved PLA with chloroform, after the ultrasonic dispersion of HA in a little chloroform for 15 min, put the dispersed HA to the PLA solution, and then stirred for 4 h. Second, we weighed 20% continuous and aligned CF bundles in volume fraction, and then dip the CF into the mixture solution made in the first step to form the pre-impregnating belt. Solvent was volatilized later. In order to decrease the alveoli in the specimens, we took the following steps: cold pressing in room temperature for 10 min, then hot pressing at 170°C, 40 MPa for 20min, transfer the specimens to the cold press machine for cooling to the room temperature. The sample we obtained indicated that the carbon fiber

paralleled along the length and mechanical properties tests were carried out perpendicularly from the fiber direction. The flexural strength and modulus of the intact CF/HA/PLA composites and after *in vitro* exposure were measured by the three-point bending method, using a universal material testing machine (SANS-CMT 4204，SANS，China) at room temperature. The distance between supports was 30 mm. The testing speed was 1 mm/min. Samples for three-point bend tests had dimensions of approximately 2 mm × 3 mm × 40 mm.

The shear strength of the intact CF/HA/PLA composites and after *in vitro* exposure, was measured by means of a tool, which was constructed by modifying the standard BS 2782, Method 340B [24]. The tool consisted of two parts, which were joined together by the implant (Fig.2.1). During the test, the parts were pulled apart using a universal material testing machine operating at a crosshead speed of 10 mm/min. Thus the implant, resting in a drill hole, was cut into three pieces perpendicular to the long axis of the rod. The size of the drill hole was chosen such that it was easy to push the test sample through the holes in the tool (approximate diameter of the drill hole 0.1 mm larger than the test sample). The shear strength was calculated using

$$\tau_s = \frac{2F_{\max}}{\pi d^2} \qquad (2.1)$$

where τ_s is the shear strength (MPa), $F_{\max}$ the maximum force recorded (N) and the d the diameter of the rod (mm). Samples for shear tests were cylindrical with an approximate diameter of 3 mm and height of 30 mm.

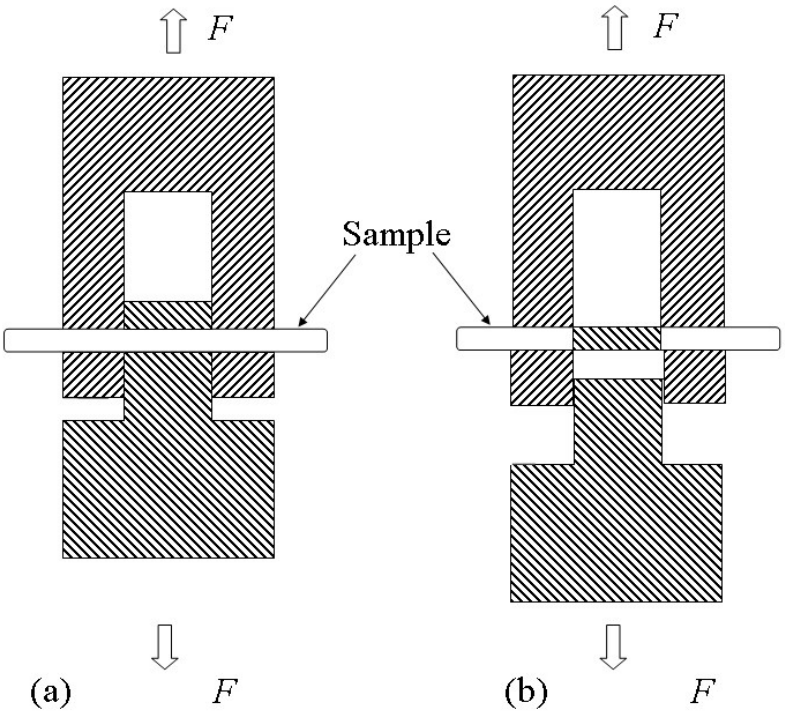

Fig.2.1 A schematic cross-sectional drawing of the shear strength test. During the test, the two parts of the hardened stainless steel test tool were pulled apart such that the test sample resting in a drill hole, and initially joining the parts of the tool together (a), was cut into three pieces perpendicular to the long axis of the rod (b).

2.2.3 Degradation *in vitro* of CF/PLA/ HA

Several specimens of CF/HA/PLA composites (mass ratio of HA to PLA 15/85) were chosen. Phosphate buffer solution (PBS) with the initial pH value of 7.40 was prepared. Put the specimens into the PBS (10ml PBS for each specimen). After that, specimens were stored in the 37°C incubator, replaced PBS once a week. 5 specimens have been chosen every few weeks, to determine the mechanical properties of CF/HA/PLA by a universal material testing machine in the whole 3 months. Meanwhile, the variation of pH values, water uptake and mass loss of CF/HA/PLA composites were studied by the general ways as below: number 10 specimens and weigh each specimen with electronic balance, soak them in 100ml PBS, change PBS once a week. Measure the pH value of PBS with pH meter and weigh the wet weight of specimens regularly. After that, vacuum dry the specimens at 50°C until constant weight is attained. Record the constant weight. Then calculate the water uptake and mass loss of the 10 specimens and average them. The formula for calculating the water uptake W_A and mass loss W_L are shown as follows:

$$W_A\,\% = 100\,(\,W\mathrm{s} - W\mathrm{r})\,/\,W\mathrm{r} \qquad (2.2)$$

$$W_L\,\% = 100\,(\,W_0 - W\mathrm{r})\,/\,W_0 \qquad (2.3)$$

where, W_s is the wet weight, W_r the constant weight, W_o the initial weight.

2.2.4 Scanning electron microscopy (SEM)

SIRION FE-SEM (FEI, Netherlands) was used to characterize the surface morphology of the CF before and after oxidized by HNO_3 and the microstructures of the intact CF/HA/PLA composites and after *in vitro* exposure.

2.3 Results and discussion

2.3.1 Surface treatment of CF

SEM photos of CF before and after oxidized by HNO_3 show that it increases the surface roughness of CF, as presented in Fig.2.2. Its smooth surface has been shift to be grooved one after the oxidation. According to the analysis of specific surface area, the specific surface area of oxidized CF is 1.172m^2/g nearly 5 times than the previous one untreated (0.289m^2/g). Thus increase the contact area and mechanical interlocking effect between CF and matrix.

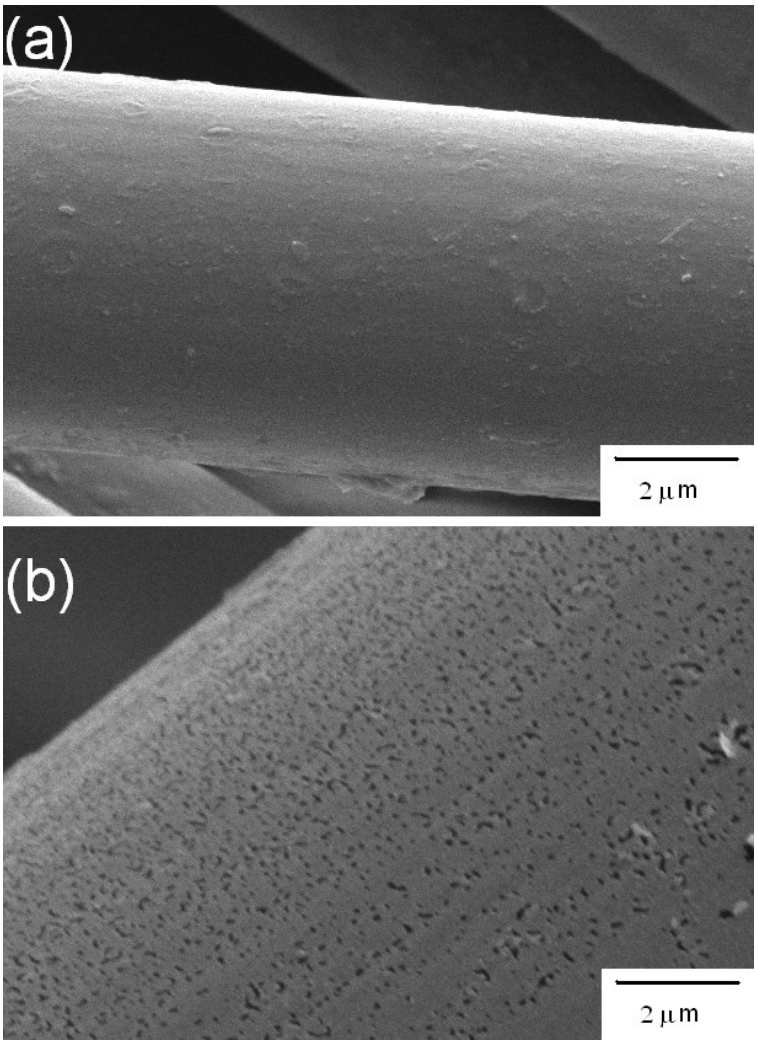

Fig.2.2 SEM photos of CF before (a) and after (b) oxidized by HNO_3

2.3.2 Flexural properties and degradation *in vitro* of CF/HA/PLA

Fig.2.3 shows the dependence of flexural strength (a) and flexural modulus (b) on HA mass fraction of CF/HA/PLA composites. Fig.2.3 (a) suggests that when HA mass fraction is low, flexural strength increases as HA mass fraction rises, it reaches the maximum when HA mass fraction is 15%, after reaching the peak, flexural strength decreases as HA mass fraction rises. In the Fig.2.3 (b), In the Fig.2.3 (b), it illustrates that the flexural modulus performed the similar trend to Fig.2.3 (a). The trend is nearly the same as the literatures reported, but the flexural strength is almost 4-6 times that of the HA/PLA composite [14]. The reason why the strength of this kind of composite is higher than HA/PLA is that CF plays the role of strengthening material. HA could increase the flexural modulus because of its rigidity, on the other hand, with the joining in of HA particles, the interfacial bonding between CF and matrix weakens, and it increases the opportunity to form defects in the composite. When the added HA mass fraction reaches a certain amount, the dispersal of HA particles reduces, which causes the stress concentration, and finally the flexural strength to decrease. The mutual competition of the two mechanisms leads to the trend that the flexural strength and flexural modulus increase in the beginning and decrease after the peak.

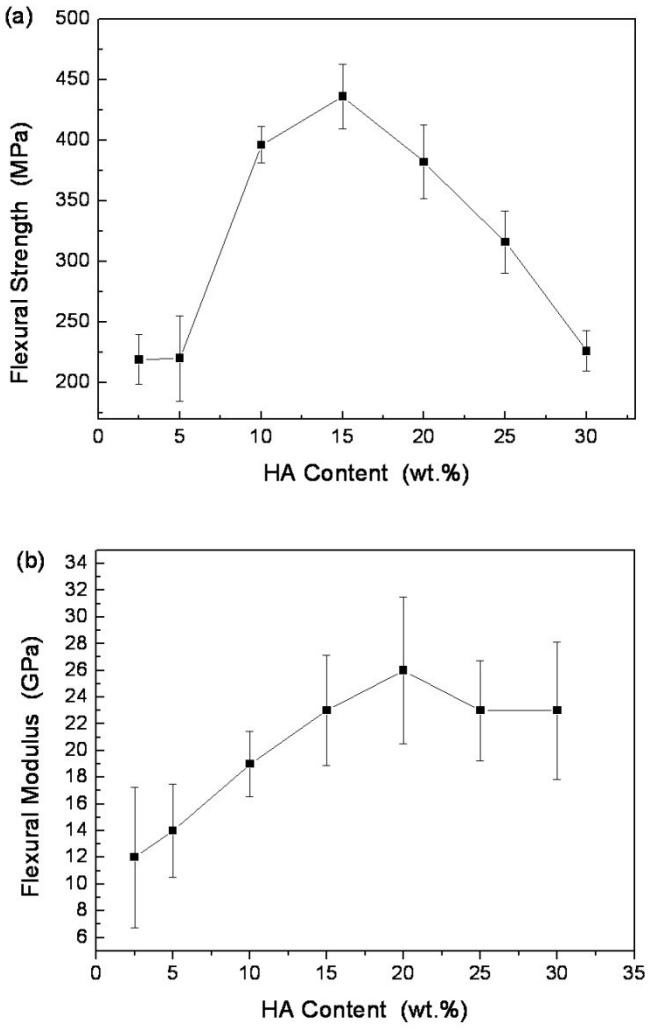

Fig.2.3 The dependence of flexural strength (a) and flexural modulus (b) on HA mass fraction of CF/HA/PLA composites（CF volume fraction 20%）

The *in vitro* degradation behavior of the ternary composite is mainly investigated in following aspects: the strength of the material, the attenuation of the modulus, mass loss, water absorption and the change of the pH value during soaking in certain solution.

Fig.2.4 shows the changes in flexural strength and flexural modulus of CF/HA/PLA during the degradation in phosphate buffer solution (PBS) at 37°C, it can be observed that as the degradation goes, the flexural strength and flexural modulus decrease continuously. With the 12-week degradation, the flexural strength decrease 10% from 430 MPa to 388 MPa, the flexural modulus decrease 13%, from 22 GPa to 19 GPa. The CF/HA/PLA composite can maintain the excellent mechanical properties for several months, which is conducive to the regeneration of bone tissue at an early period.

Fig.2.5 indicates changes in water uptake and mass loss during the degradation in PBS at 37°C. It represents that with the extension of degradation, water uptake and mass loss both increase, after degradation for 12 weeks, water uptake is 5% while mass loss is only 1.6%.

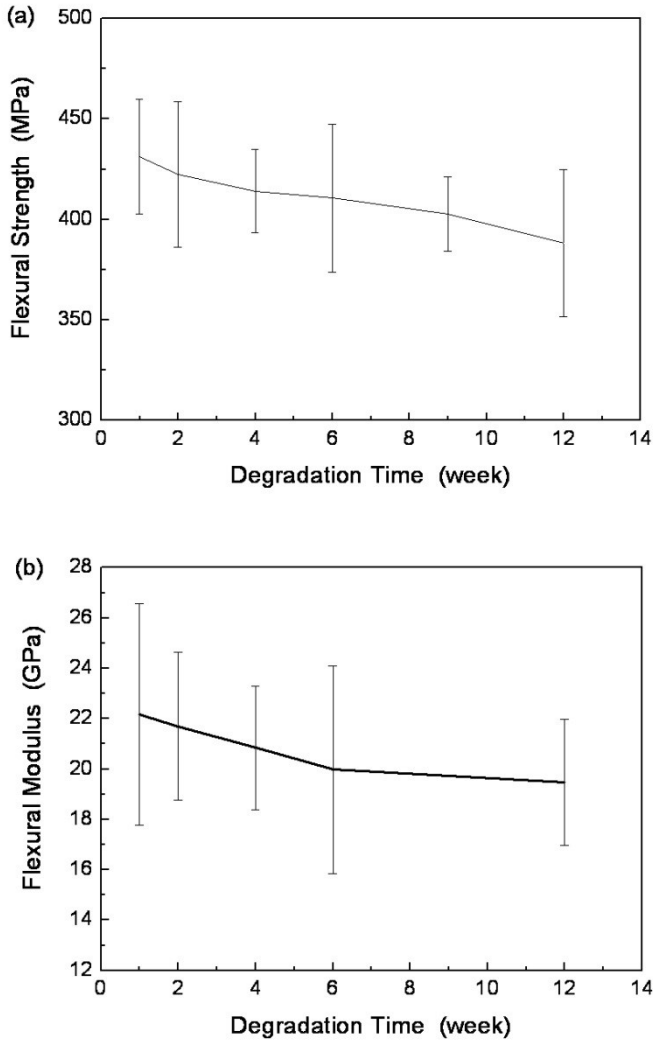

Fig.2.4 Changes in flexural strength and flexural modulus of CF/HA/PLA during the degradation in phosphate buffer solution (PBS) at 37°C (CF volume fraction 20%, HA/PLA mass ratio 15/85)

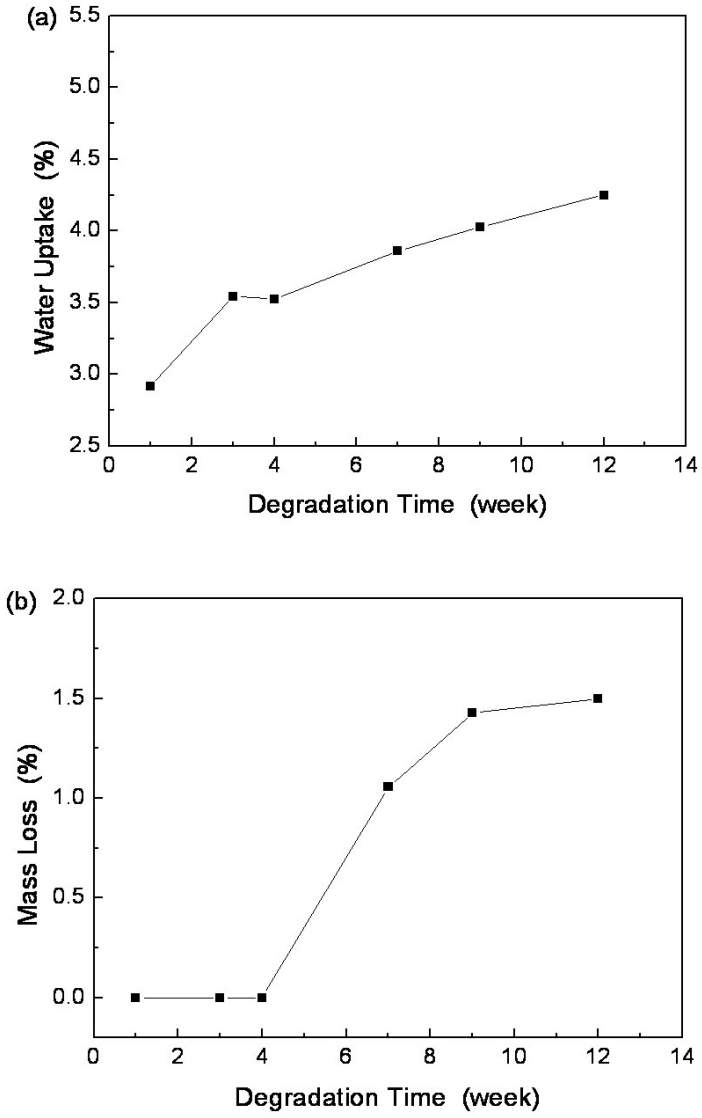

Fig.2.5 Changes in water uptake (a) and mass loss (b) during the degradation in PBS at 37°C (CF volume fraction 20%, HA/PLA mass ratio 15/85)

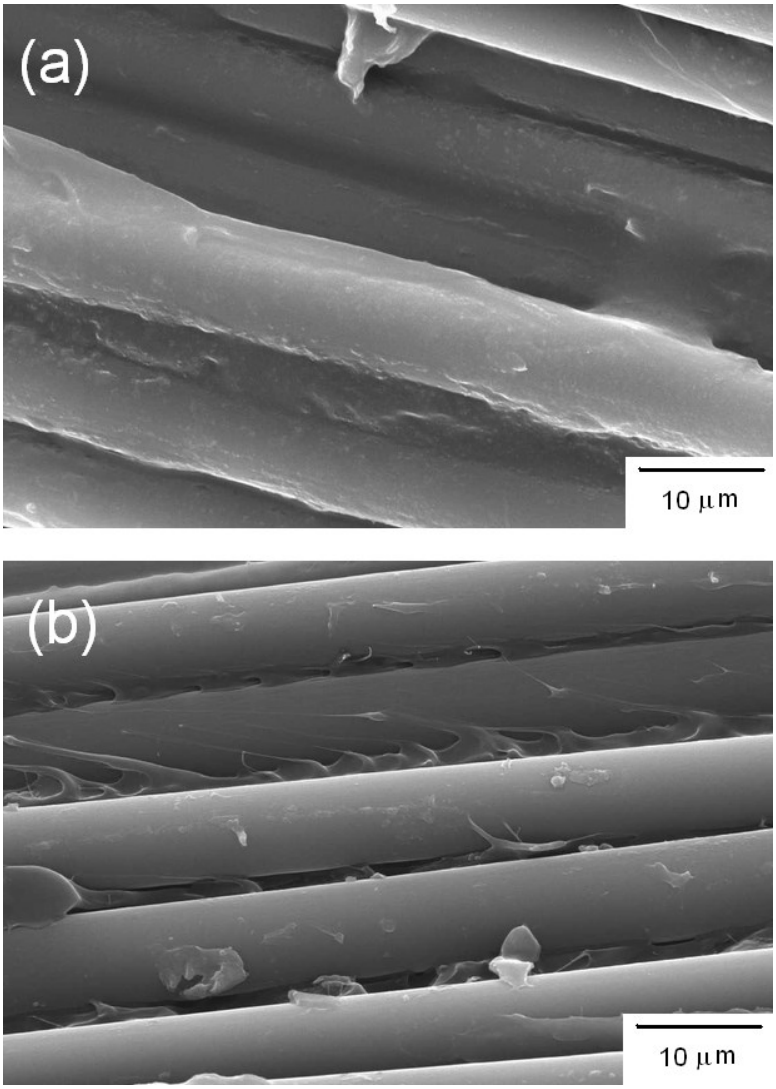

Fig.2.6 Longitudinal profile (fiber direction) SEM photos of the CF/HA/PLA composites degraded in PBS for 1 week (a) and 12 weeks (b) (CF volume fraction 20%, HA/PLA mass ratio 15/85)

Fig.2.6 shows SEM photos of the CF/HA/PLA composites degraded in PBS for 1 week (a) and 12 weeks (b). It shows that CF and matrix combine closely in the first week, but then there're gaps between CF and matrix after soaking 12 weeks. Interfacial degradation is the most important factor of the strength falling. SEM photos would prove it. As the interfacial bonding strength declines, the strength of the material declines. Between CF and matrix, there exists interface where the water uptake effects take place. Water diffuses to the inner of the composite easily through the interfaces because of capillarity. These account for the continuously increasing water uptake. Fig.2.7 states changes in pH values of PBS during the degradation. The pH value of PBS during the whole degradation drops less than 0.1, shows that the alkaline of HA neutralize the acid degrades from PLA.

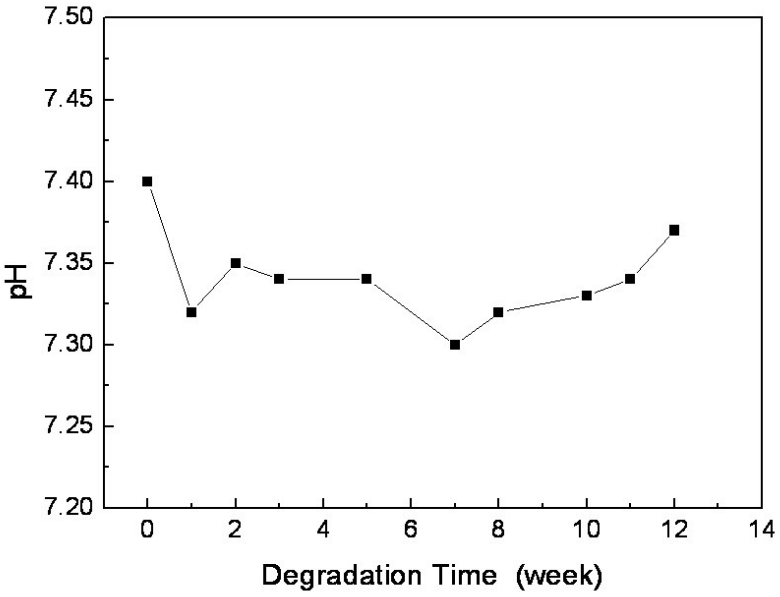

Fig.2.7 Changes in pH values of PBS during the degradation time (CF volume fraction 20%, HA/PLA mass ratio 15/85)

2.3.3 Shear strength and degradation *in vitro* of CF/HA/PLA

We can see in the Fig.2.8 that the dependence of shear strength on HA content of CF/HA/PLA composites is similar to the dependence of flexural strength on HA content of CF/HA/PLA composites. When HA mass fraction is low, flexural strength increases as HA mass fraction rises, it reaches the maximum when HA mass fraction is 20%, after that, flexural strength decreases as HA mass fraction rises.

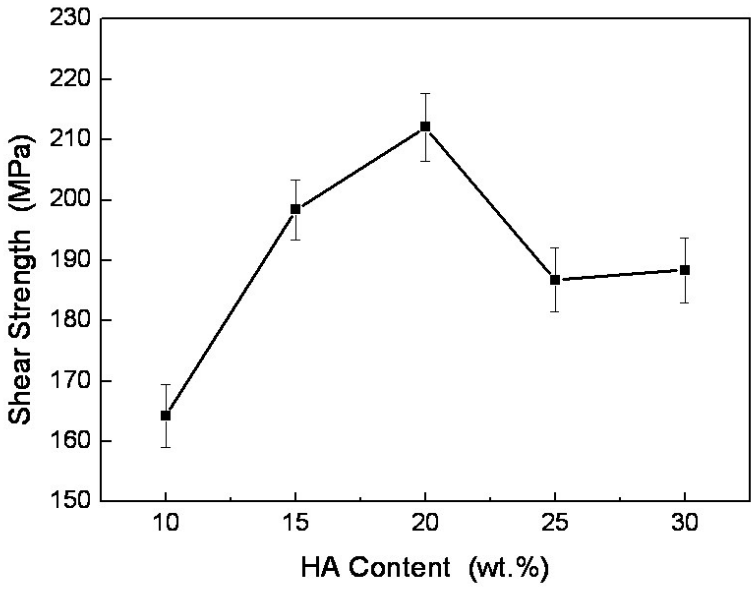

Fig.2.8 The dependence of shear strength on HA mass fraction of CF/HA/PLA composites （CF volume fraction 20%）

Fig.2.9 shows the changes in shear strength during the degradation in PBS at 37°C of the CF/HA/PLA composites. It indicates that after degradation for a week, it is saturated in water uptake, the shear strength drops by 100 MPa. With the degradation carrying on, there is no obvious change in the shear strength, keeping it at the level of 190 MPa. Fig.2.10 shows SEM photos of fracture surfaces of the CF/HA/PLA composites degraded in PBS for 1 week (a) and 12 weeks (b) after shear strength test. We can see that the PLA matrix has not been degraded after soaking in PBS for one week. However the PBS immersing takes place in the interface and leads to the strength decline. After immersing for 12 weeks, as degradation of some PLA matrix, we can observe that there are gaps between CF and PLA, as shown in Fig. 10 (b). Because there are no changes on CF, the shear strength of the composite levels off in the later degradation.

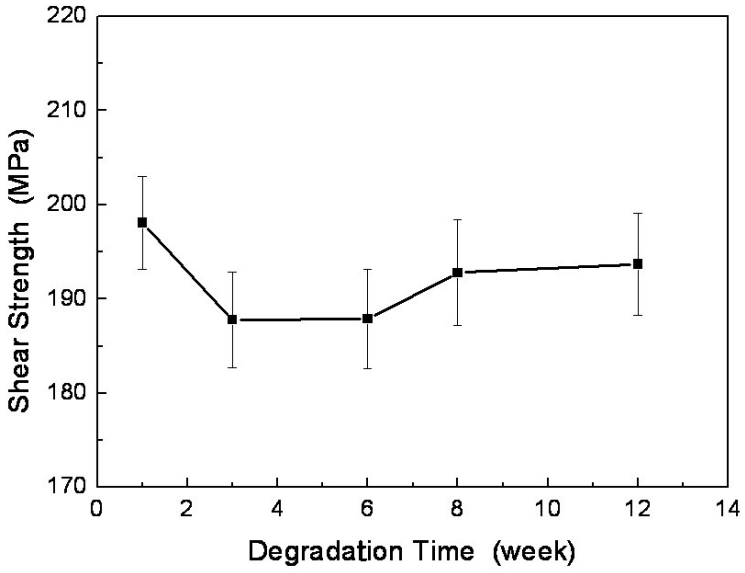

Fig.2.9 Changes in shear strength during the degradation in PBS at 37°C of the CF/HA/PLA composites (CF volume fraction 20%, HA/PLA mass ratio 15/85)

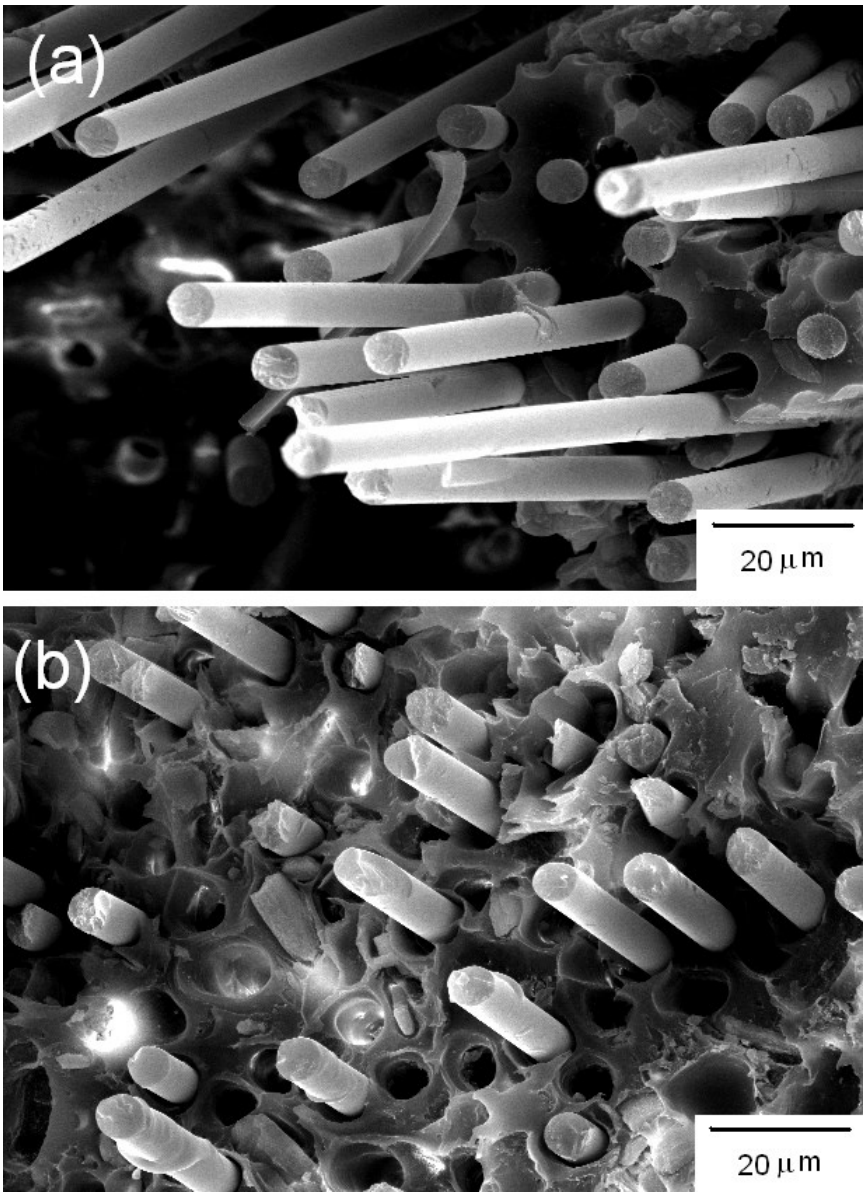

Fig.2.10 SEM photos of fracture faces of the CF/ PLA/HA composites degraded in PBS for 1 week (a) and 12 weeks (b)

2.4 Conclusions

CF reinforced HA/PLA degradable biomaterial is prepared by hot pressing a prepreg which consisting of PLA, HA and CF. The composites have good mechanical properties. A peak showed in flexural strength, flexural modulus and shear strength aspects, reaching up 430 MPa, 22 GPa, 212 MPa respectively, as the HA content increased. Degraded *in vitro* for 3 months, the flexural strength and flexural modulus of the CF/HA/PLA fell 13.2% and 5.4% respectively, while the shear strength of the CF/HA/PLA composites remains at the 190 MPa level. Water uptake increased to 5%, while the mass loss rate was 1.6%. The SEM photos showed that there were gaps between the PLA matrix and CF after degradation, which was considered as hydrolysis of PLA at interface. The pH values of the PBS dropped less than 0.1. That's because the alkaline of HA neutralize the acid degrades from PLA, which can prevent the body from the acidity harm.

References:

1. LD. Anderson. Treatment of ununited fractures of the long bones; compression plate fixation and the effect of different types of internal fixation on fracture healing. J. Bone Joint Surg. Am. A 47, 1965, 191.

2. T. Terjesen, Bone healing after metal plate fixation and external fixation of the osteotomized rabbit tibia. Acta Orthop. Scand. 55, 1984, 69.

3. T. Terjesen, K. Apalset, The influence of different degrees of stiffness of fixation plates on experimental bone healing. J. Orthop. Res. 6, 1988, 293.

4. C. Uchikura, J. Hirano, F. Kudo, K. Satomi, T. Ohno, Comparative study of nonbridging and bridging external fixators for unstable distal radius fractures. J. Orthop. Sci. 9, 2004, 560.

5. T.L. Huang, C.K. Huang, J.K. Yu, F.Y. Chiu, H.T. Liu, C.L. Liu, T.H. Chen, Operative treatment of intra-articular distal radius fractures using the small AO external fixation device. J. Chin. Med. Assoc. 68, 2005, 474.

6. ZB. Luklinska, W. Bonfield, morphology and ultrastructure of the interface between hydroxyapatite-polyhydroxybutyrate composite implant and bone. J. Mat. Sci. Mat. Med. 8, 1997, 379.

7. JY. Rho, L. Kuhn-Spearing, P. Zioupos, Mechanical properties and the hierarchical structure of bone. Med. Eng. Phys. 20, 1998, 92.

8. T. Yasunaga, Y. Matsusue, T. Furukawa, Y. Shikinami, M. Okuno, T. Nakamura, Bonding behavior of ultrahigh strength unsintered hydroxyapatite particles/poly(L-lactide) composites to surface of tibial cortex in rabbits. J. Biomed. Mat. Res. 47, 1999, 412.

9. RK. Kulkarni, EG. Moore, AF. Hegyeli, F. Leonard, Biodegradable poly(lactic acid) polymers. J. Biomed. Mater. Res. 5, 1971, 169.

10. S. Vainionpää, P. Rokkanen, P. Törmälä, Surgical applications of biodegradable polymers in human tissues. Prog. Polym. Sci. 14, 1989, 679.

11. Y. Matsusue, S. Hanafusa, T. Yamamuro, Y. Shikinami, Y. Ikada, Tissue reaction of bioabsorbable ultra high strength poly (L-lactide) rod. A long-term study in rabbits. Clin. Orthop. 317, 1995, 246.

12. JE. Devin, MA. Attawia, CT. Laurencin, Three-dimensional degradable porous polymer-ceramic matrices for use in bone repair, J. Biomater. Sci. Polymer. Edn. 7, 1996, 661.

13. KG. Marra, JW. Szem, PN. Kumta, PA. DiMilla, L.E. Weiss, In vitro analysis of biodegradable polymer blend/hydroxyapatite composites for bone tissue engineering. J. Biomed. Mater. Res. 47, 1999, 324.

14. NC. Bleach, KE. Tanner, M. Kellomaki, P. Tormala, Effect of filler type on the mechanical properties of self-reinforced polylactide–calcium phosphate composites, J. Mat. Sci. Mat. Med. 12, 2001, 911.

15. V. Maquet, AR. Boccaccini, L. Pravata, I. Notingher, R. Jérôme, Porous poly(alpha-hydroxyacid)/bioglass composite scaffolds for bone tissue engineering. I: Preparation and in vitro characterization. Biomaterials 25, 2004, 4185.

16. R. Zhang, PX. Ma, Poly(α-hydroxyl acids)/hydroxyapatite porous composites for bone-tissue engineering. I. Preparation and morphology, J. Biomed. Mater. Res. 44, 1999, 446.

17. Y. Shikinami, M. Okuno, Bioresorbable devices made of forged composites of hydroxyapatite (HA) particles and poly L-lactide (PLLA). Part II: practical properties of miniscrews and miniplates, Biomaterials 22, 2001, 3197.

18. T. Kasuga T, H. Maeda, K. Kato, Preparation of poly(lactic acid) composites containing calcium carbonate (vaterite), Biomaterials 24, 2003, 3247.

19. ZK. Hong, PB. Zhang, CL. He, Nano-composite of poly(L-lactide) and surface grafted hydroxyapatite: Mechanical properties and biocompatibility, Biomaterials 26, 2005, 6296.

20. J. Chlopek , A. Morawska-Chochol , G. Bajor , M. Adwent , A. Cieslik-Bielecka , M.

Cieslik , D. Sabat, The influence of carbon fibres on the resorption time and mechanical properties of the lactide–glycolide co-polymer. J. Biomater. Sci. Polymer. Edn. 18, 2007, 1355.
21. Y. Hojo, Y. Kotani, M. Ito, K. Abumi, T. Kadosawa, Y. Shikinami, A. Minami, A biomechanical and histological evaluation of a bioresorbable lumbar interbody fusion cage. Biomaterials 26, 2005, 2643.
22. AK. Al-Shawi, SP. Smith, GH. Anderson, The use of a carbon fiber plate for periprosthetic supracondylar femoral fractures. J Arthroplasty 17, 2002, 320.
23. B. Czajkowska, M. Blazewicz, Phagocytosis of chemically modified carbon materials, Biomaterials 18, 1997, 69.
24. BS 2782: Part 3: Methods 340A and 340B (British Standards Institution, London, 1978).

Chapter 3

Relationship between Annealing and Shape Memory Effect of Shape Memory Polyurethane

3.1 Introduction

Shape memory polymers (SMPs) are polymers with the ability to store and recover strains on the order of several hundred percent when subjected to a particular thermomechanical cycle [1]. Different from shape memory alloys (SMAs) [2], the shape memory effects in SMPs is predominantly an entropic phenomenon [3]. It can be induced by various external stimuli, such as heat [4], light [5], electric field [6], magnetic field [7] or radiation [8] to return to its original shape. Polyurethane (PU) is one of the most important materials in the SMP family. SMPs' attractiveness mainly lies in their ease of processing and low cost [9]. PU shape memory polymers are generally synthesized following common synthetic routes such at reacting diisocyanates and polyols with a diol or triol as a crosslinker [10]. Shape recovery is one of the indexes that people are concerned about for evaluating shape memory effect. In general, polyurethane SMPs are considered to consist of 'netpoints' and molecular switches. Netpoints are hard segments acting as a fixed phase under a certain thermomechanical cycle, which are assumed as crystalline, glassydomains, chain entanglements or chemical cross-links. The soft segments work as a reversible phase, which actively move as the thermal energy is inputted [11].

Meanwhile, annealing of polymer is a kind of second process wherein the polymer is brought to a certain temperature, kept for a certain time and then cooled to room temperature [12]. Annealing is also one of the ways to modify the material properties of thin films to the preferred properties [13, 14]. For example, the crystallinity of the polymer can be adjusted from annealing, as degree of crystallinity is determined by structural regularity of the polymer. Annealing can decrease the regularity if the polymer has a regular structure, which is obtained from external forces. In contrast, it also could increase the regularity if the initial structure is disordered. There are also some other researchers doing investigation on effects of annealing with morphology change [12]. Thus, annealing treatment of shape memory polyurethane (SMPU) and the

influence of annealing on shape memory recovery are quite important.

In this study, thermal annealing experiments of SMPU film were conducted to investigate how annealing affects film length by time. After that, annealing and thermomechanical cycle experiments with different time combination were conducted to discover the relationship between annealing and shape recovery effect of this film. Finally, experiments with precisely controlled annealing time and thermal recovery time from calculation were carried out in order to validate our assumption.

3.2 Experiments

3.2.1 Experiment for annealing: equipment and process

Uniaxially oriented SMPU film with approximately 50μm thickness was prepared. Raw materials which were thermoplastic polyurethane pellets with glass transition temperature (Tg) of 55°C (MM5520) were provided by SMP Technologies Inc. SMPU film was produced by cast film extrusion process in a factory. For experiment, films with size of 250mm × 15mm were cut from film rolls. Figure 3.1 is the photo of SMPU film roll and film cut from the roll.

Fig. 3.1 Photo of a roll of polyurethane shape memory polymer produced by cast film extrusion process and some film slices cut from the roll.

For annealing, water bath was used to control the temperature. A ceramic glass hotplate (IKA C-MAG HP7) which can provide constant temperature to water bath was used. A digital thermometer was also used to measure water bath temperature. PU has high polarity, which makes it have high surface tension and high surface free energy. Moreover, the SMPU film that used for experiment was oriented during manufacturing. So at relatively high temperature, film curls and sticks together to reduce surface free energy. Therefore in our experiment, one end of the film is clipped by a binder clip. The other end wounds round a small piece of balsa wood. Balsa wood was chosen because of its low density ($0.11 g/cm^3$), which could reduce the influence from constraints to the greatest extend when taking out film from water bath. Binder clip is tired with a string for the ease of taking out film. Length change of the red mark at different time intervals is measured by microscope. Annealing test equipment is illustrated in Fig.3.2. Annealing was carried out at 60°C, 65°C and 70°C, for each temperature, 3 repetitions were done to see if the results had good repeatability. Length change of the film was recorded. Curve fitting was done.

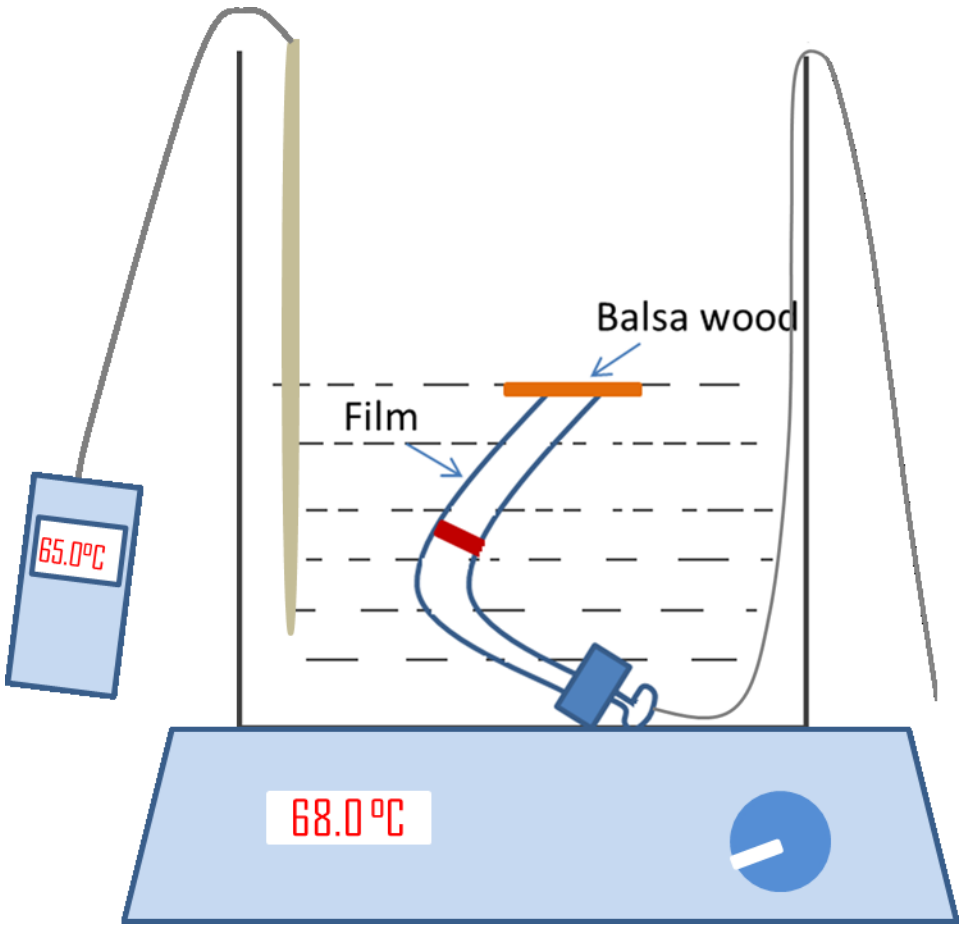

Fig. 3.2 Sketch of annealing process of SMPU film.

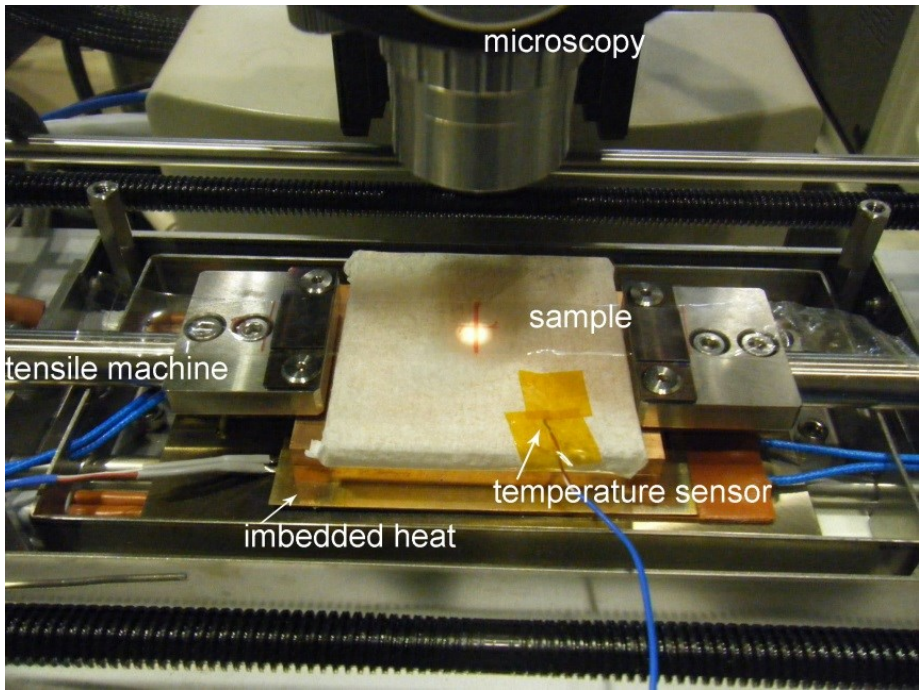

Fig. 3.3 Device for shape memory thermomechanical cycles.

3.2.2 Experiment for thermomechanical cycle: equipment and process

For thermomechanical cycles, a tensile test machine with heating system imbedded was used and a microscope was used for recording the length change of the film as seen in Fig.3.3.

Thermomechanical cycles were done by fixing the film in the tensile machine, followed by increasing temperature to 65°C. Temperature of the film was measured by a digital infrared temperature sensor (KEYENCE, FT) and keeping at the same temperature by the imbedded heat. After that, approx. 15(±1) % of elongation was applied to the film. Length was measured by microscope (KEYENCE, VHX). Then temperature was cooled down to room temperature at 27°C within 10min with two small fan motors. Shape recovery was carried out at 65°C water bath for 10s.

3.2.3 Experiment for annealing and shape memory effect

4 samples with different annealing time and shape recovery time were prepared. Table 1 shows annealing time and shape recovery time of these 4 samples. For example, sample No.2 went through a 10s of annealing first, followed by a thermomechanical cycle with recovery time of 20s. This experiment was repeated three times. After that the relationship of annealing and shape recovery was revealed.

Table 3.1 Annealing time and shape recovery time of 4 samples.

Sample number	Annealing time [s]	Elongation ratio in thermomechanical cycle	Shape recovery time [s]
1	/	15%	30
2	10	15%	20
3	20	15%	10
4	30	15%	/

3.2.4 Experiment designed for controlling shape change ratio

From the curving fitting equation and the relationship of annealing and shape recovery, the time which is needed for a desired length change ratio can be calculated. Annealing and thermomechanical cycle experiments with controlled time that calculated from equation were conducted and results were analyzed.

3.3 Results and discussion

3.3.1 Result of annealing

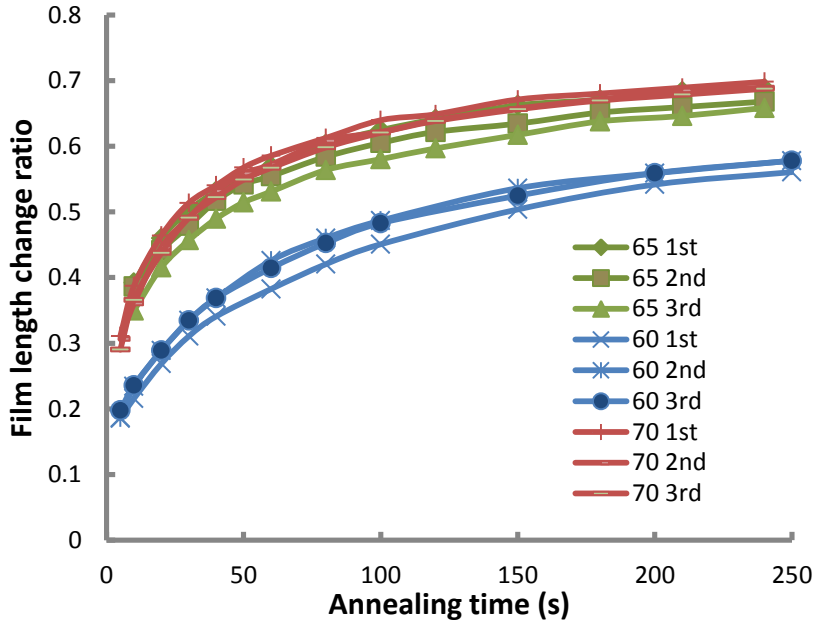

(a) Film length change ratio with respect to annealing time. 3 repetitions for each temperature.

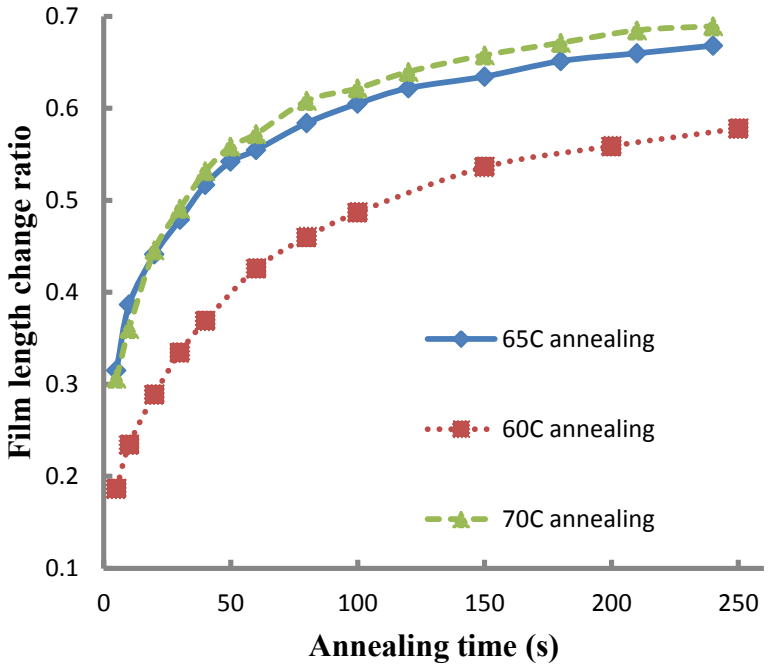

(b) Figure of film length change ratio with respect to annealing time. Curve in the middle of 3 repetitions is shown here.

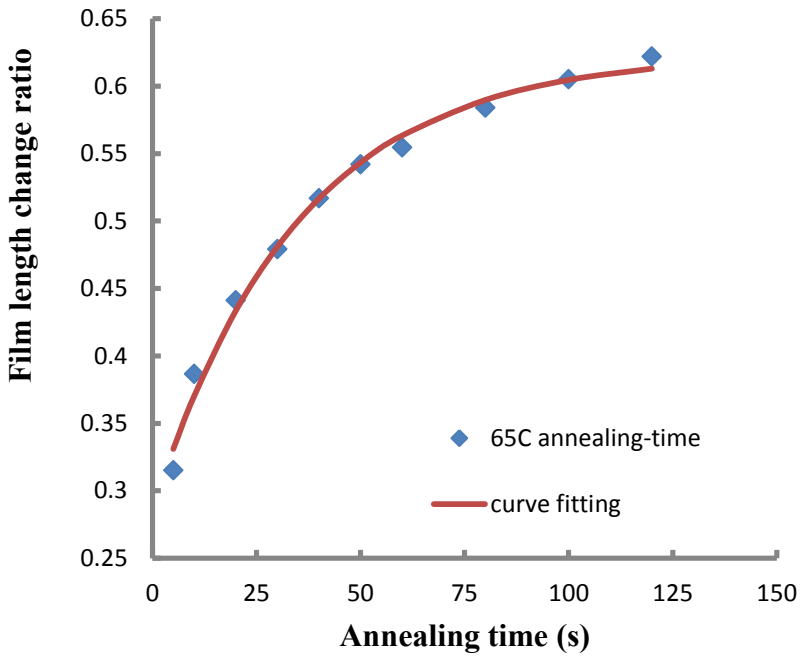

(c) Curve fitting to length change ratio-annealing curve by least square

Fig. 3.4 (a) (b) Relationship of film length change ratio and annealing time at 60°C, 65°C, and 70°C. 3 repetitions and the one in the middle. (c) Least square fitting to the curve at 65°C.

Fig. 3.4 (a) shows the relationship of length change ratio and annealing time at three different temperatures. The intermediate curve for each temperature is shown in figure 3. 4 (b).

Length change ratio here (as well as shape change ratio and shape recovery ratio) is defined as the following equation:

$$r = \frac{lo - la}{lo} \qquad (3.1)$$

where *r* is length change ratio, *lo* is the original length and *la* is the length afterwards.

3 repetitions were done for each temperature. It can be seen that annealing property at one temperature is quite stable. For temperature at 60°C, length change ratio was in the region from nearly 0.2 to 0.58, while for both 65°C and 70°C, this was from nearly 0.3 to 0.68. It can be seen that in this temperature region, the higher the temperature, the larger the length change ratio. This is obvious because high temperature provides more energy for polymer chains to relax from orientation. Curves for 65°C and 70°C are close. That means polymer chains are reaching their

relaxation limit at these temperatures. It is also shown that with the increasing of time, length change ratio caused by annealing becomes stable. It is because with the time increasing, residual strain from material manufacturing process decreases.

Fig. 3.4(c) shows the curve fitting of length change ratio *r* as a function of time *t*. This was done by least square method.

Equation from curve fitting for 65°C is as following:

$$r = -0.3379*e^{(-0.0287*t)} + 0.6237 \quad (3.2)$$

where r is length change ratio, and *t* is annealing time.

From this equation, length change ratio at any annealing time can be calculated.

3.3.2 Result of thermomechanical cycles

3 samples were used to carry out thermomechanical cycle test for SMPU film, shown in Fig. 3.5. Y axis is normalized film length, which means dividing all the lengths by its original length. Shape recovery time was 10 seconds. 3 samples had shape change ratio of 23.4%, 28.9% and 27.1% respectively. This shows there is good reproducibility among these 3 samples in length change ratio.

Minor difference can come from: Sample difference, for example, slightly difference of internal residual stress or samples were from different batches; Error in operating experiment, such as controlling heating temperature, recovery temperature and recovery time.

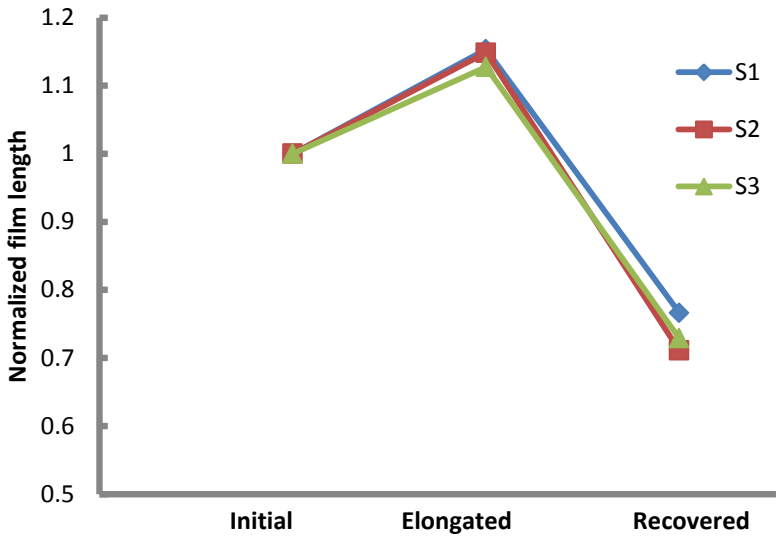

Fig. 3.5 Film length changes of 3 samples in one thermomechanical cycle after normalizing.

3.3.3 Relationship between annealing and shape memory effect

Fig. 3.6 shows a total length change ratio of 4 samples described in Table 3.1. Here a total length change ratio is defined by the difference between lengths before annealing and after thermomechanical cycle divided by the original length before annealing. From this figure, we can see that no matter it was pure annealing or pure shape memory thermomechanical cycle, or different time combination of annealing and shape recovery, as long as they are the same in total time, the length change ratio is almost the same. This means, for this SMPU, length change from annealing and shape memory effect at the same temperature is the same. This can be understood as follows: annealing is a process that by heating up material, polymer chains relax from the low entropy state created by the stretch from manufacturing, follows by returning to stable high entropy state if annealing time is long enough. Meanwhile, the mechanism of shape memory effect is similar, by stretching at relatively high temperature above the glass transition temperature and cooling down, it temporarily stores energy of low conformational entropy state in molecular chains between crosslinking nodes, when heating above the glass transition temperature, stored strain recovers via an increase in the network free volume, chain rearrangement, and finally the recovery of a stable high entropy state in polymer.

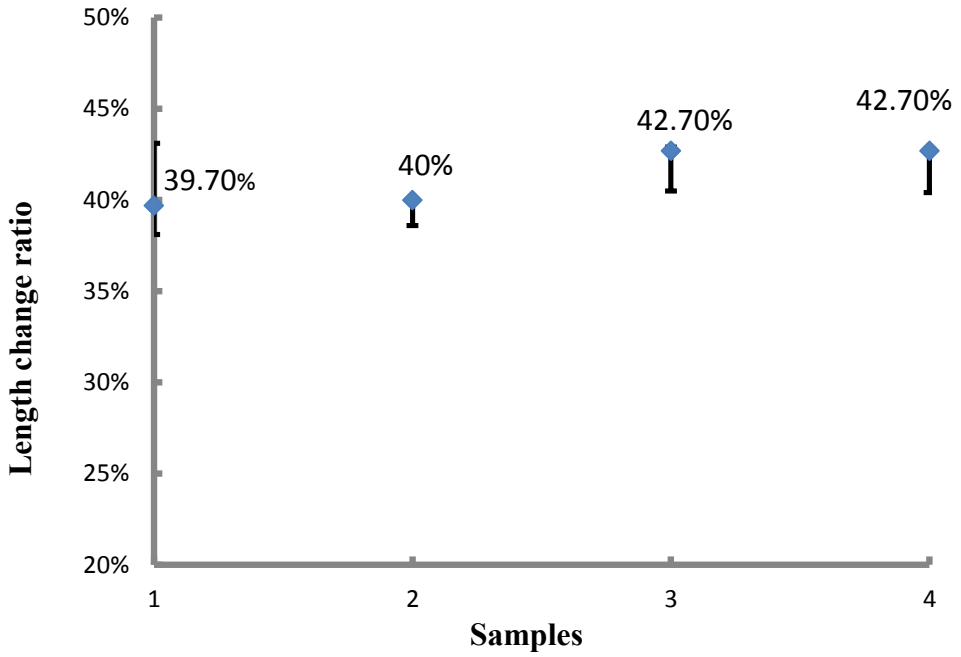

Fig. 3.6 Total length change ratio of 4 samples. The figure shows results from 3 replications of experiment.

3.3.4 Result of shape change ratio controlling experiment

From results above, we can assume, it is a feasible and easy way to control the shape recovery ratio of SMP by controlling the annealing level, which is of interest in various parts of fields where SMP is used. Here is an example of controlling shape recovery ratio at 45% by annealing time. We assume original length as *lo*, length after pure annealing is *la*, and then final length includes elongation after annealing is (1+0.15) × *la*.

$$\frac{lo-(1+0.15)\times la}{lo} = 0.45 \qquad (3.3)$$

So $la = \frac{1-0.45}{1+0.15} \times lo = 0.478\ lo$

For annealing without elongation:

Length change ratio is $r = \frac{lo-la}{lo} = \frac{lo-0.478lo}{lo} = 0.522$

Substitute r as 0.522 into equation 3.2, we can calculate the time needed to have a shape recovery ratio of 45% is 41.7s.

We performed experiments of 3 samples with a total processing time of 41.7s and length change during the experiments was measured. We can see all 3 samples closely reached to a length change ratio of 45%. This proves that shape recovery ratio of shape memory polyurethane can be designed by annealing.

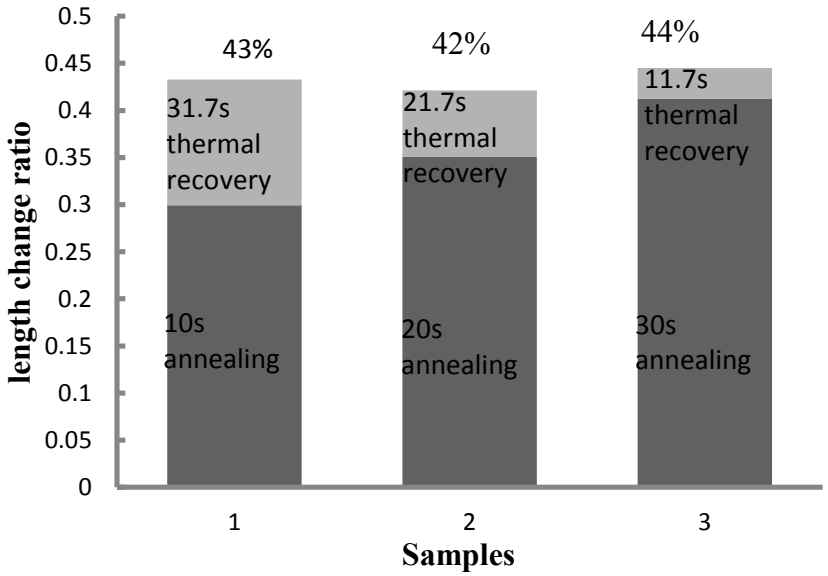

Fig. 3.7 All three samples with same total annealing time and thermal recovery time reach the designated shape recovery ratio.

3.3.5 Discussion from molecular point of view

SMP has a working principle of storing energy in molecular chains during cooling down in thermomechanical cycle and releasing energy when temperature increases. As written in the introduction part, it is a process of changing of entropy in materials. For annealing, it is same. Energy is stored in molecules during orientation in manufacturing, kept when the products cool down, and released during annealing. Therefore, the processes of annealing and shape memory are, in essence, the same. In this article, only temperature at 65°C was discussed. Results need to be further discussed if temperature is changed when crystallization occurs.

3.4 Conclusions

(1) We studied length change of SMPU film under annealing at 3 different temperatures. From the results it can be seen that different temperatures lead to different length change ratio at same time interval.

(2) By comparing the length change ratio from annealing and thermomechanical effect of SMPU, we concluded that annealing and shape memory effect had same effect on length change of SMPU.

(3) We also demonstrated that for obtaining a certain length change ratio of SMPU, result is same if the total processing time of annealing and thermomechanical recovery is same as the pure annealing time which is needed for the equivalent effect. Therefore, we conclude that we can control shape recovery ratio of SMPU by adjusting annealing time.

References:

1. K. Otsuka, C. M. Wayman (Eds.), Shape Memory Materials, Cambridge University Press, New York, 1998.

2. H.E. Karaca, E. Acar, G.S. Ded, B. Basaran, H. Tobe, R.D. Noebe, G. Bigelow, Y.I. Chumlyakov, Shape memory behavior of high strength NiTiHfPd polycrystalline alloys, Acta. Mater. 61, 2013, 5036.

3. H, Lu, Y. Yao, WM Huang, J. Leng, D. Hui. Significantly improving infrared light-induced shape recovery behavior of shape memory polymeric nanocomposite via a synergistic effect of carbon nanotube and boron nitride, Composites Part B. 62, 2014, 256.

4. H. Meng, G, Li. A review of stimuli-responsive shape memory polymer composites, Polymer 54, 2013, 2199.

5. A. Lendlein, H. Jiang, O. Junger, R. Langer, Light-induced shape-memory polymers, Nature 434, 2005, 879.

6. Y. Liu, H. Lv, X. Lan, J. Leng, S. Du, Review of electro-active shape-memory polymer composite, Compos. Sci.Technol. 69, 2009, 2064.

7. A.M. Schmidt, Electromagnetic activation of shape memory polymer networks containing magnetic nanoparticles, Macromol. Rapid Commun. 27, 2006, 1168.

8. GM. Zhu, QY. Xu, GZ. Liang, HF. Zhou, Shape-memory behaviors of sensitizing radiation-crosslinked polycaprolactone with polyfunctional poly(ester acrylate), J. Appl. Polym. Sci. 95, 2005, 634.

9. PT Mather, XF Luo, I.A. Rousseau, Shape memory polymer research, Annu. Rev. Mater. Res. 39, 2009, 445.

10. I.A. Rousseau, Challenges of shape memory polymers: A review of the progress toward overcoming SMP's limitations, Polym. Eng. Sci. 48, 2008, 2075.

11. J. Leng, X. Lan, Y. Liu, S. Du, Shape-memory polymers and their composites: Stimulus methods and applications, Prog. Mater, Sci. 56, 2011, 1077.

12. M. Talukdar, Effect of annealing on morphology of thermotropic liquid crystalline polyesters, Int. J. Res. Rev. Appl. Sci. 4, 4, 2010, 405.

13. Y. Fu and J. R. Lakowicz, Spectroscopy, A closer look at polymer annealing, Nature, 472, 2011, 178.

14. J. Petermann, M. Miles, H. Gleiter, Growth of polymer crystals during annealing, J. Macromol. Sci. B. 12, 3, 1976, 393.

Chapter 4
Fluorescence Spectroscopy to Detect Structural Change in PU Shape Memory Polymer with Different Thermomechanical Cycles

4.1 Introduction

Shape memory polymers (SMPs) are polymers with the ability to store and recover strains on the order of several hundred percent when subjected to a particular thermomechanical cycle [1]. They are a kind of important smart polymers, which have the advantages of light weight, good processability, low cost, high shape deformability, high shape recoverability and tailor-able switch temperature [2-6]. SMPs have found broad applications in smart textiles [7], intelligent medical devices [8, 9], heat shrinkable packages for electronics [10], sensor and actuators [11], self-deployable structures in space craft [7, 12], etc. Among various SMPs, shape memory polyurethanes (PUs) are receiving much attention for their excellent shape memory effect and the potential to be used as self-repairing or biomaterials [13]. Shape memory PUs basically consist of two phases, hard segments which act as the physical crosslink, and soft segments which act as reversible phase. When reversible phase is heated to a softened state, SMPs would be deformed. The deformation would be fixed when it is cooled to a hardened state. After that, original shape is recovered at above glass transition temperature (Tg), which is due to the strong dipole-dipole interaction among the hard segments components [14]. There are researches show that shape memory effect is closely related to some structural change, e.g. the amount of hard segments would affect the ratio of recovery and low content of hard segments would lead to the recovery incomplete [15]. Shape recovery ratio is one of the key factors when designing SMPs. Therefore, we attempted to develop a method to investigate the change of shape recovery ratio, assuming it is attributed to structural change in polymer.

Laser confocal scanning microscopy (LCSM) is a microscopic technique that can provide fluorescent information of specimen layer-by-layer. It has become an invaluable tool for a wide

range of investigations in biological, medical and material sciences for imaging and analyzing thin sections in fixed specimens ranging in thickness up to 100 micrometers [16]. Modern instruments usually are equipped with 3-5 laser systems controlled by high-speed acousto-optic tunable filters, which is an electro-optical device that functions as an electronically tunable exciation filter to simultaneously modulate the intensity and wavelength of multiple laser lines from one or more sources [17]. Also it coupled with photo multipliers which are capable of examining fluorescence emission ranging from 400nm to 750nm [18]. Spectral imaging detection systems further refine the technique by enabling the examination and resolution of fluorophores with overlapping spectra as well as providing the ability to compensate for auto-fluorescence [16]. The main advantage of using an LCSM to measure fluorescence is that it is primarily sensitive to the response coming from an in-focus plane of the specimen, by the design of pinhole. Meanwhile focus on thickness direction can be adjusted. Thus layer-by-layer fluorescence information can be gained.

The confocal principle in LCSM is schematically presented in figure below.

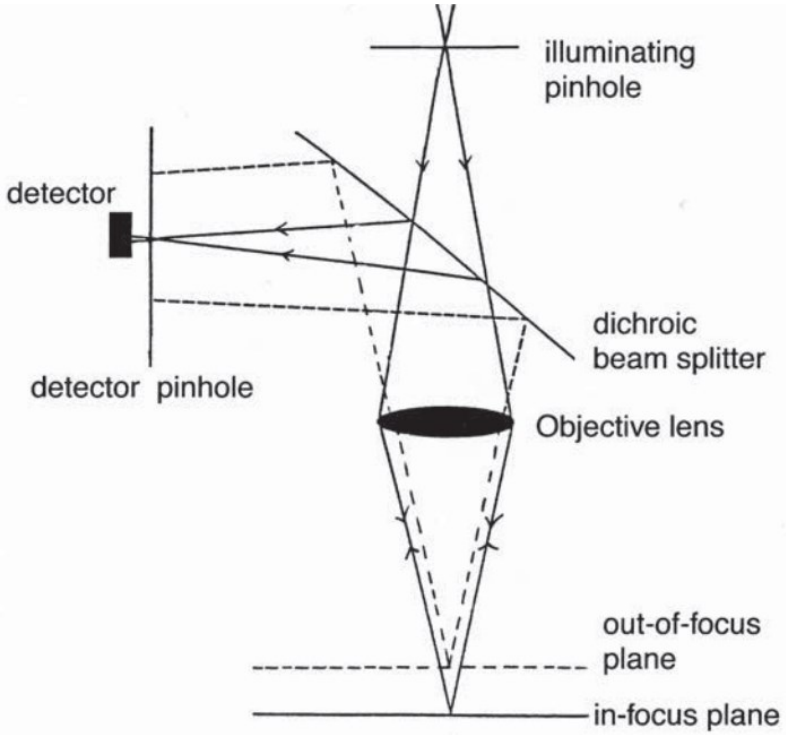

Fig.4.1 Schematic diagram of the optical pathway and principal components in a laser confocal scanning microscopy [19].

Coherent light emitted by the laser system (excitation source) passes through a pinhole aperture that is situated in a conjugate plane (confocal) with a scanning point on the specimen and a second pinhole aperture positioned in front of the detector (a photomultiplier tube). As the laser is reflected by a dichromatic mirror and scanned across the specimen in a defined focal plane, secondary fluorescence emitted from points on the specimen (in the same focal plane) pass back through the dichromatic mirror and are focused as a confocal point at the detector pinhole aperture [16].

Light originating from in-focus plane can pass the pinhole freely, whereas light coming from out-of-focus planes is blocked by pinhole. In the measurement, fluorescence dyes are excited by laser light. Fluorescence from that focalized point can be detected. By controlling laser's focus points inside specimen, fluorescent intensity at different depths in the specimen can be detected [19].

Previous researches show that LCSM is useful in characterizing material properties such as surface morphology [20, 21, 22], structure development in polymers [23]. Moreover researches of detecting material properties by bonding fluorescent dye molecules to target material by chemical reaction such as done by Goda et al. [24] or by immersion of fluorescent dye in fluid/fluid system [25] were reported. We attempt to apply this technology to detect structural change by immersing fluorescent dye in fluid/solid system using LCSM.

The present study developed a method based on fluorescence spectroscopy in order to detect the difference of shape recovery ratio (length change ratio in this work) of PU shape memory polymer film. Fluorescence intensity change was measured by LCSM. Comparing results between the samples with different thermomechanical cycles, we discuss the effectiveness of the fluorescence spectroscopy to detect the structural change of shape memory polyurethane (SMPU).

4.2 Experiment

4.2.1 Thermomechanical cycles for PU shape memory polymer

We investigated the effectiveness of fluorescence spectroscopy using SMPU film with different thermomehcanical cycles. This study used uniaxially oriented SMPU film with approximately 50μm thickness. Raw materials which were thermoplastic polyurethane with glass transition temperature of 55°C (MM5520) were provided by SMP Technologies Inc.

For thermomechanical cycle, a tensile test machine with heating system imbedded was used and a microscopy was used for recording the shape change of the film. Thermomechanical cycles were done by fixing the film in the tensile machine, then temperature was increased to 65°C and kept there by the imbedded heat. After that, approx. 15(±0.5)% of elongation was applied to the film. Then temperature was cooled down to room temperature at 27°C within 10min. Shape recovery was carried out at 65°C in water bath. Samples with 1 and 5 thermomechanical cycles were prepared.

4.2.2 DSC test

Differential scanning calorimetry (DSC) provides a rapid method for determining polymer Tg and degree of crystallinity based on the heat required to melt the polymer, if crystallized. In our experiment, DRG-50 (Shimadzu) was used for measuring sample weight. DSC-50 and DTG-50 (Shimadzu) were used for DSC test.

Samples after 0, 1, 5, 10 thermomechanical cycles were prepared and analyzed over the temperature range from ambient (about 17°C) to 200°C. A heating rate of 10°C/min was used with atmospheric air around the sample. Since thermal history of a polymer affects the measured degree of crystallinity, these samples were evaluated “as received”.

4.2.3 Fluorescent solution and immersion

After thermomechanical cycle(s), one group of samples (with 0, 1, 5 thermomechanical cycles) were soaked in pyranine ethanol solution (5μg/ml), another group (same samples) were soaked in uranine ethanol solution (5μg/ml), both were at room temperature (21°C) for 30min. Pyranine and uranine in ethanol solution have peak absorption wavelength at about 400nm [26] and 493nm [27] respectively. Our experiment values of peak emission wavelength of pyranine and uranine are 437nm and 522nm. After specimens were taken out, both surfaces were rinsed by ethanol twice. Whereafter, surfaces were dried by paper. The basic principle of our method is we immerse the fluorescence dyes into the sample and measure how much the fluorescence dyes can be immersed. We can consider that the difference in the amount of immersed fluorescence dyes represents some structural change in the material.

4.2.4 Laser confocal scanning microscopy measurement at different depth

The measurement of distribution of fluorescence intensity in depth direction is based on the confocal laser scanning microscopy (Olympus FV1000-D). Scanning size is 313μm by 313μm. Numerical aperture (NA) is 0.4. The excitation laser wavelength was 405nm for pyranine and 473nm for uranine. A depth of about 80μm is scanned from a bit outside of surface to inner sample and then out of the other surface. Interval from point to point is 5 to 10μm.

4.2.5 Data processing method

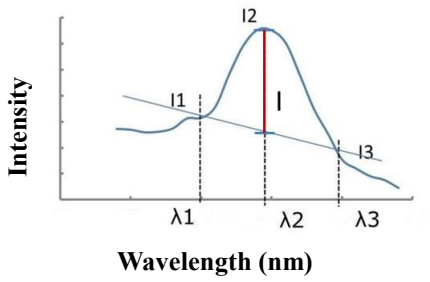

Fig. 4.2 Treatment of fluorescent spectrum. This reduces the interference of laser light scattering.

A typical spectrum that we obtain below the surface is shown in Figure 4.2. Baseline in this spectrum is not horizontal. One possible reason is that the scattering of laser incident light can

influence the spectrum when it is under the surface. Here we used a method called Fluorescence Line Height (FLH) to characterize the fluorescent intensity. λ_1, λ_3 are two wavelengths at the left and right side of spectral peak. λ_2 is the wavelength at the emission maximum. Fluorescent intensity I is defined by following equation:

$$I = I_2 - \left[\frac{\lambda_3 - \lambda_2}{\lambda_3 - \lambda_1} (I_1 - I_3) + I_3 \right] \tag{4.1}$$

where I_1, I_2 and I_3 are intensities at λ_1, λ_2 and λ_3.

From description above, fluorescent intensity at certain point can be calculated from the spectrum. If we connect fluorescence intensity in one figure, a fluorescence intensity profile in one sample can be obtained, as in sketch below.

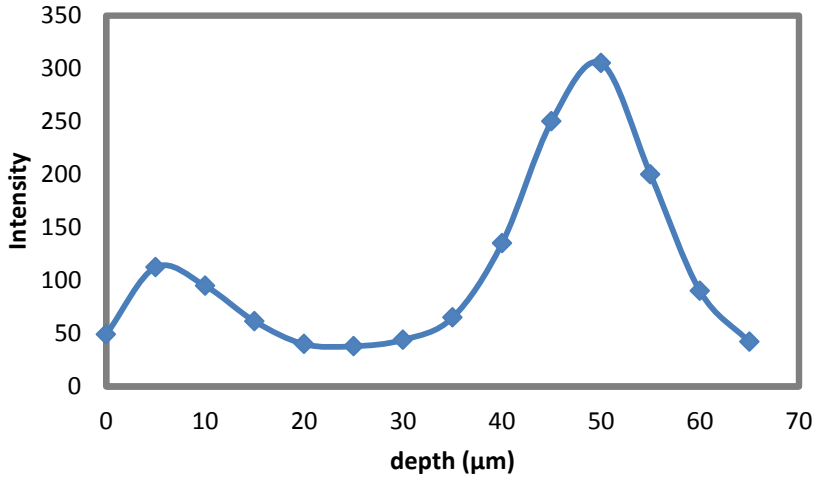

Fig.4.3 Example of intensity profile in one sample from experiment.

4.3 Results and discussion

4.3.1 Shape recovery ratio with different thermomechanical cycles

Figure 4.4 shows the results of length change ratio of the PU film with different

thermomechanical cycles. Here the length change ratio R is defined as following equation:

$$R = 1 - \frac{(l_{after} - l_{before})}{l_{before}} \tag{4.2}$$

l_{after} is the length after a cycle and l_{before} stands for the length before a thermomechanical cycle. Fig.4.4 has some points whose value exceeds 1, because length change here includes annealing during thermomechanical cycle. Annealing and shape recovery share same mechanism as reported in chapter 3 [28].

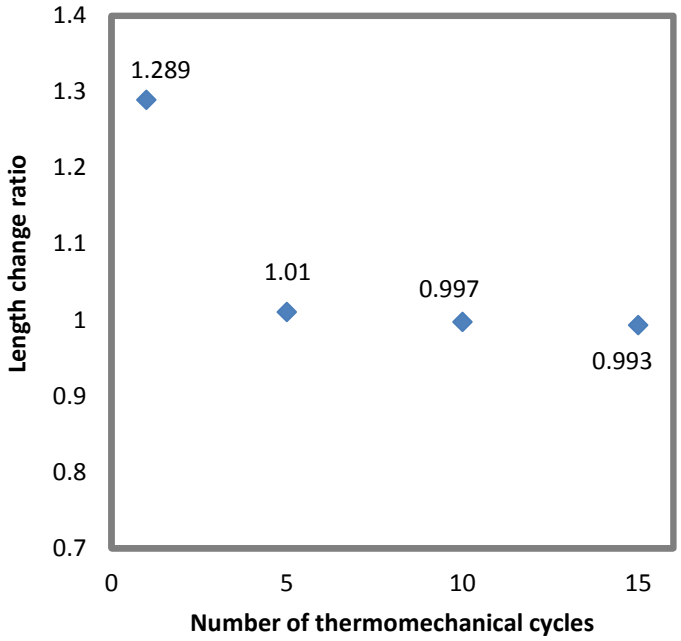

Fig.4.4 Results of shape recovery rate of the PU film with different thermomechanical cycles.

4.3.2 DSC results

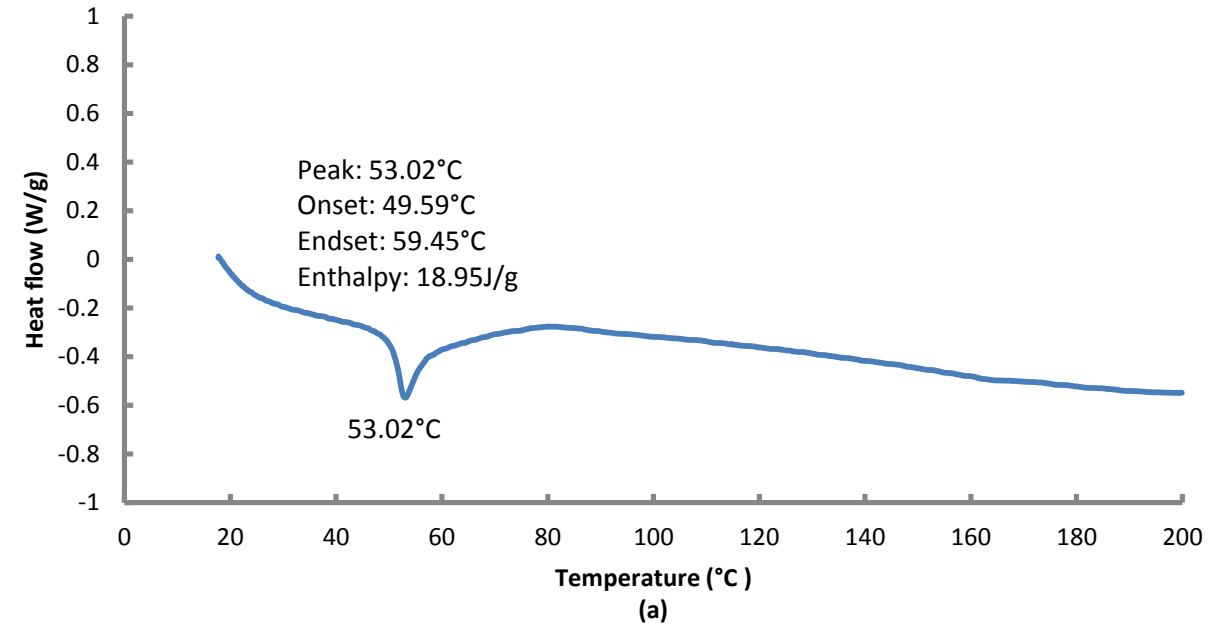

(a)

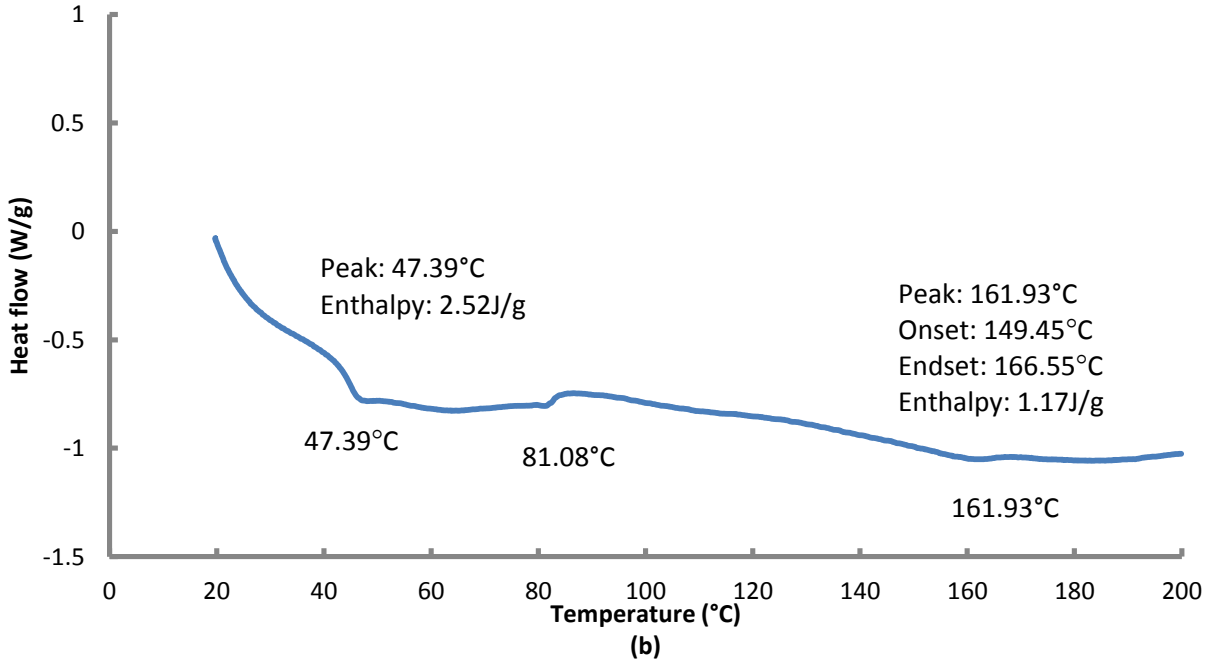

(b)

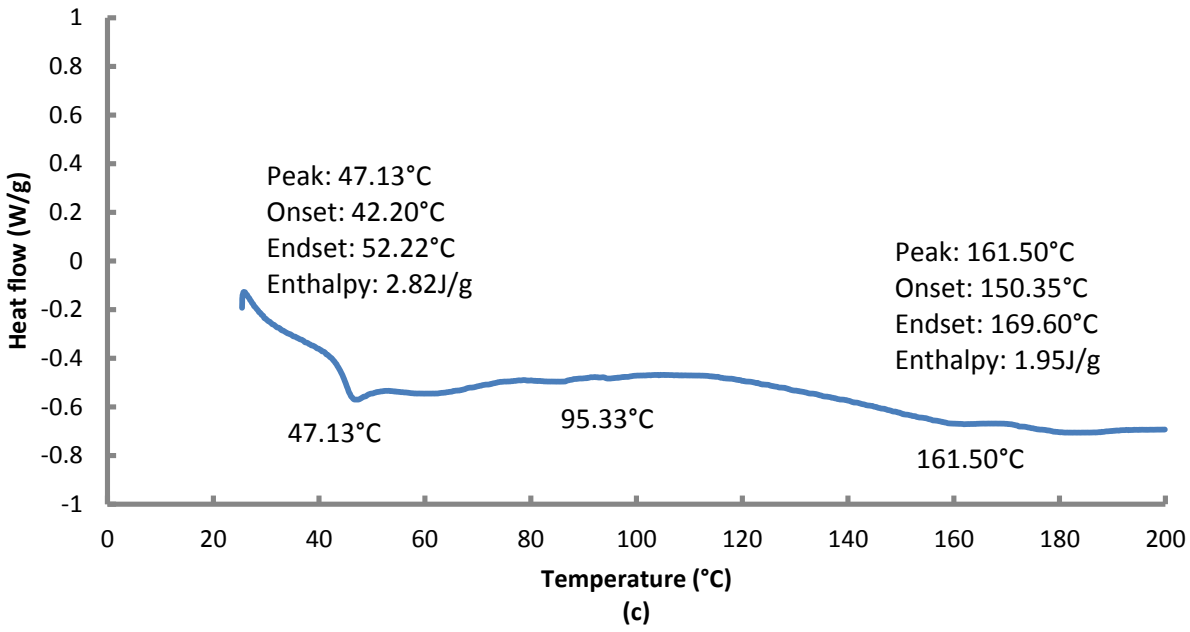

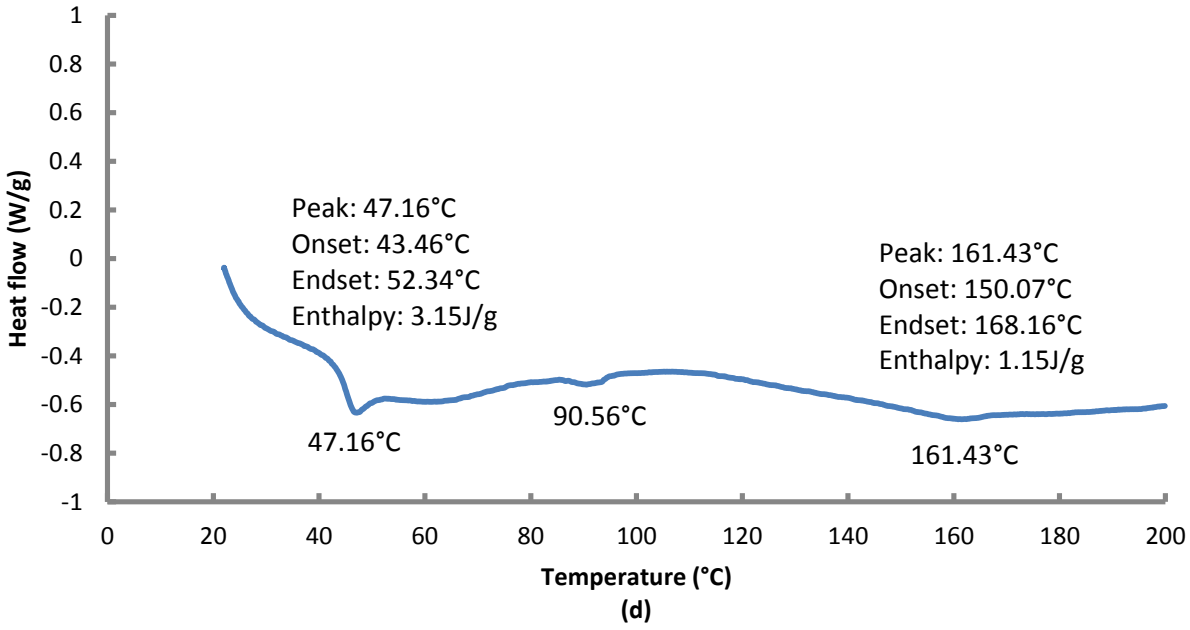

Fig. 4.5 Results of DSC measurement. (a) (b) (c) and (d) are results of samples with 0, 1, 5, 10 thermomechanical cycles respectively.

Table 4.1 DSC characterization of 4 samples.

Sample	Glass transition temperature (°C)	Crystallization temperature (°C)	Melt peak temperature (°C)	Enthalpy (J/g)
(a) 0 cycle	53.02	/	/	/
(b) 1 cycle	47.39	81.08	161.93	1.17
(c) 5 cycles	47.13	95.33	161.50	1.95
(d) 10 cycles	47.16	90.56	161.34	1.15

From Table 4.1, it can be seen that there is a difference of Tg between sample (a) which did not undergo thermomechanical cycles and sample (b), (c), (d) which underwent thermomechanical cycles. This may because of different degree of orientation between samples with and without thermomechanical cycles [29]. But from Tg, there is no difference among samples with 1, 5, 10 cycles.

Sample (a) does not have melting temperature in DSC measurement. In samples (b) (c) and (d), melting peak appears. Moreover, (b), (c) and (d) show identical in terms of melting profile. Theoretical value of the melting enthalpy of pure crystalline phase is ΔH_f = 136J/g [30]. Theoretical value of 100% crystallinity polymer may be determined by indirect methods such as extrapolation using Flory equation or other estimate methods [31].

$$\text{Crystallinity\%} = \frac{\Delta Hf - \Delta Hc}{\Delta Hf} \times 100\% \quad (4.3)$$

where ΔHc is the heat of cold crystallization.

Therefore degree of crystallinity is less than 1.5% for samples (b), (c) and (d). From here, we can see samples with 1, 5, 10 thermomechanical cycles have very small amount of crystalline, and DSC cannot show differences among these samples.

4.3.3 Fluorescence spectra of one sample

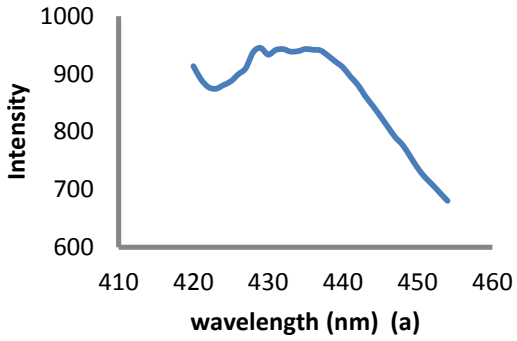

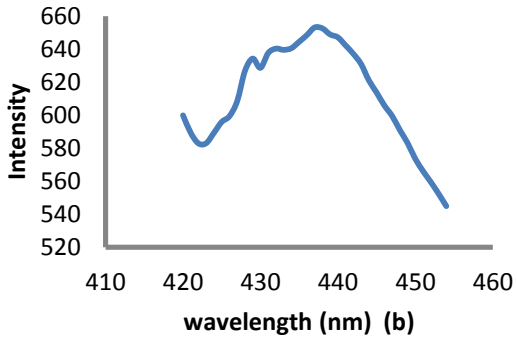

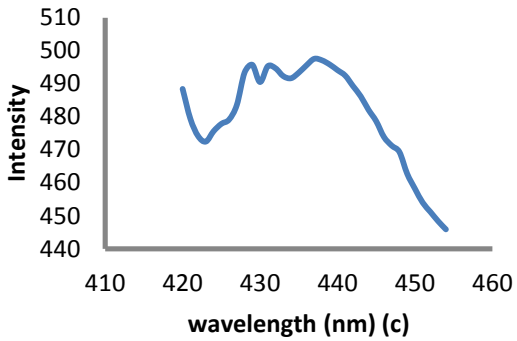

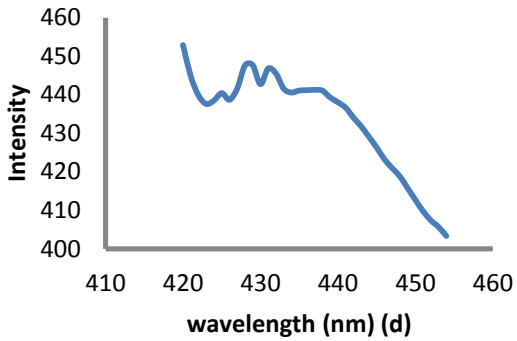

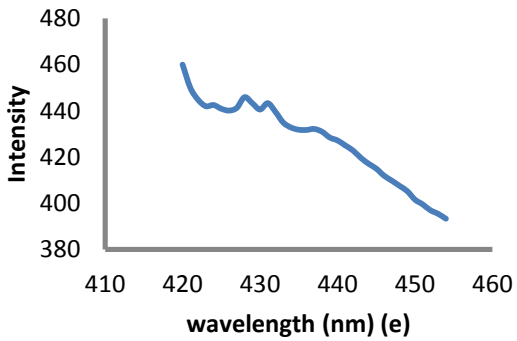

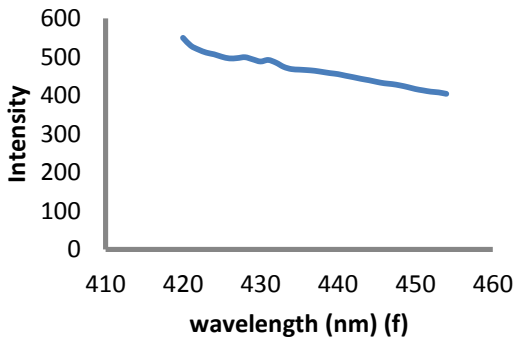

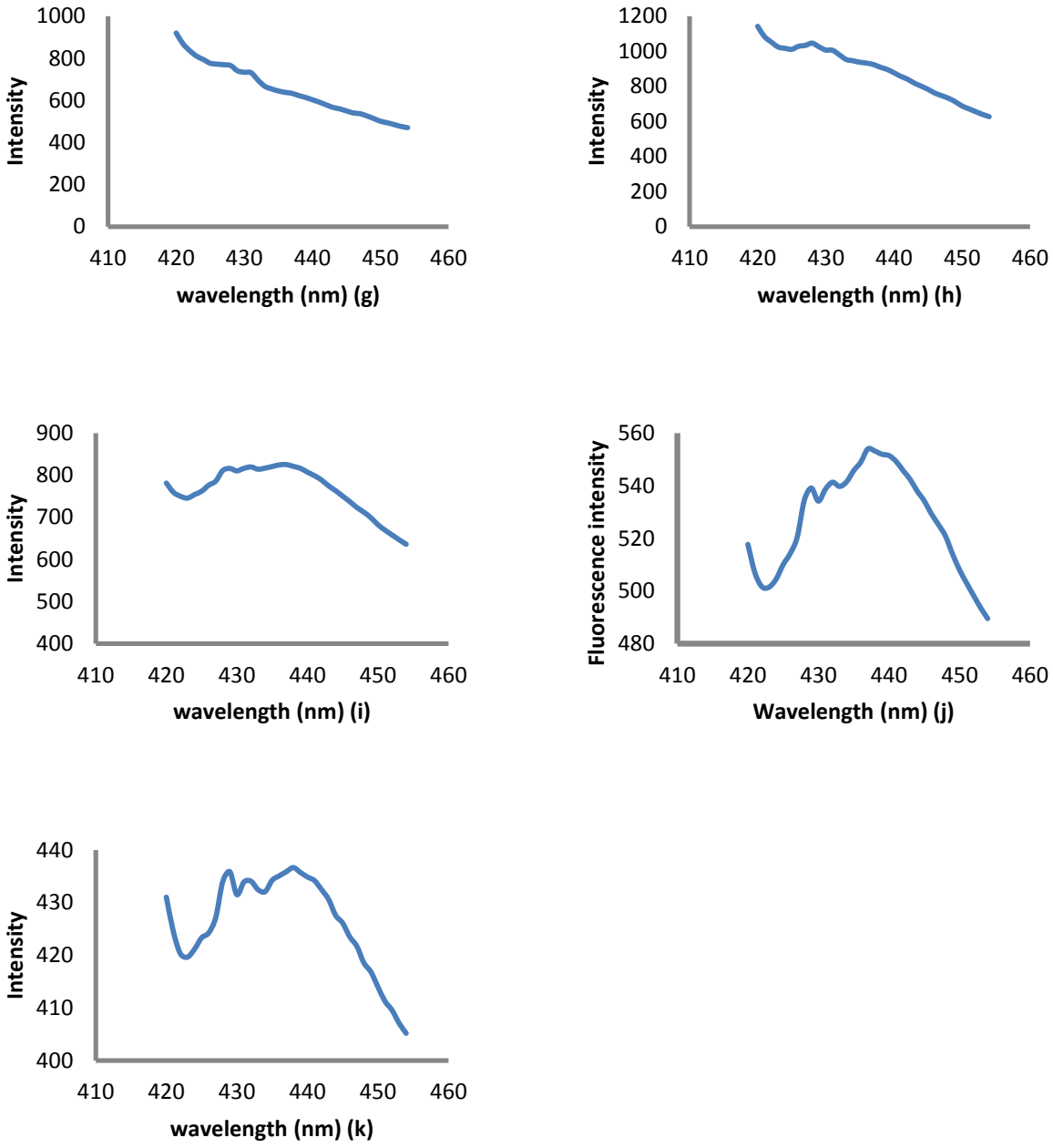

Fig. 4.6 Fluorescence spectra of SMPU sample after 1 thermomechanical cycle and immersing in pyranine solution. 11 depths in the sample from near surface to inner side were measured. 11 fluorescence spectra were obtained. (a) is most close to lower surface, and two adjacent spectra are at interval of 5μm.

This is an example of fluorescent spectra from pyranine immersed in PU shape memory film. We can see the peak emitted wavelength is at 437nm. In all the spectra from (a) to (k), there are two minor peaks appearing at wavelength of 429nm and 431nm. These two peaks can be impurities in the sample, or overlap of some other peaks which needs further discussion.

(a) and (i) which are closer to the surfaces, have larger intensity. While for (f), (g) and (h), which are about in the middle of the sample, almost do not have obvious fluorescence intensity detected. If we connect all the intensity after FLH treatment, we can obtain fluorescence intensity profile as shown in Fig. 4.7.

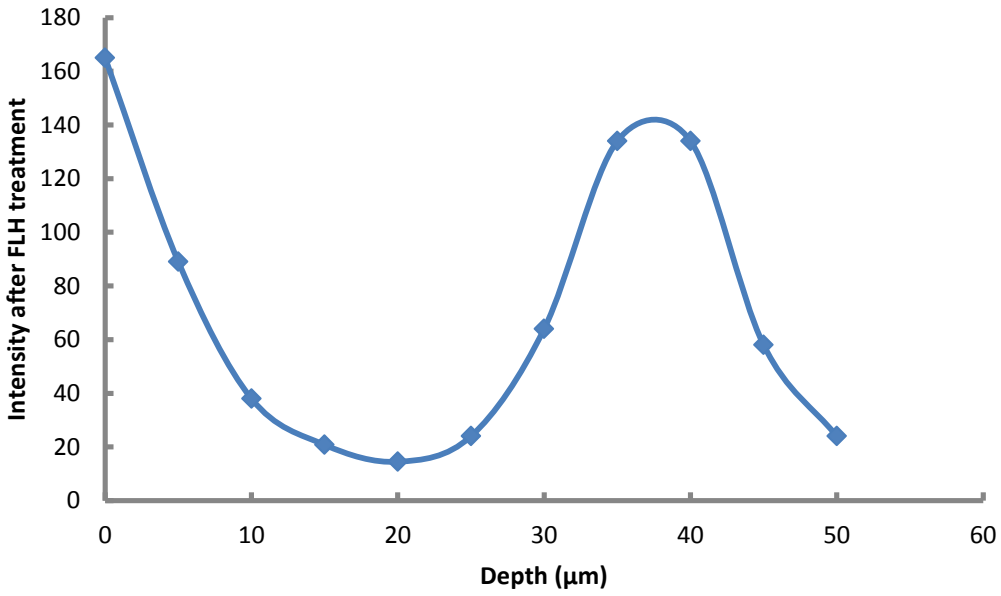

Fig. 4.7 Fluorescence intensity profile of SMPU sample after 1 thermomechanical cycle and followed by immersing in pyranine solution. Left side is where the laser light enters.

Two peaks in Fig. 4.7 correspond to two surfaces. The part between two peaks is our interest because it shows the change in immersion. Peaks at left and right have different intensity, which is considered as the result of surface facing during immersion. Also LCSM has limited detection depth range. Spectra which are closer to the surface where laser light enters are more accurate. Then as the first step, the part closer to surface where laser light enters was studied.

4.3.4 Fluorescence spectroscopy from different depth and their processing

Figure 4.8 shows the results of fluorescence spectroscopy with different thermomechanical cycles. Here peak points were discarded, because probes remained on surface influence the peak value, in addition, for pyranine, sometimes regular emission spectra on surface couldn't be obtainedIn figure 4.8, 0 on x axis doesn't mean it is surface of the sample. Figure 4.8(a) shows the distribution of fluorescence intensity in depth direction for the samples with pyranine probe under different cycles; Figure 4.8(b) shows the results with uranine probe under different cycles. In the results, we can see obvious difference of probe immersed in samples with different thermomechanical cycles.

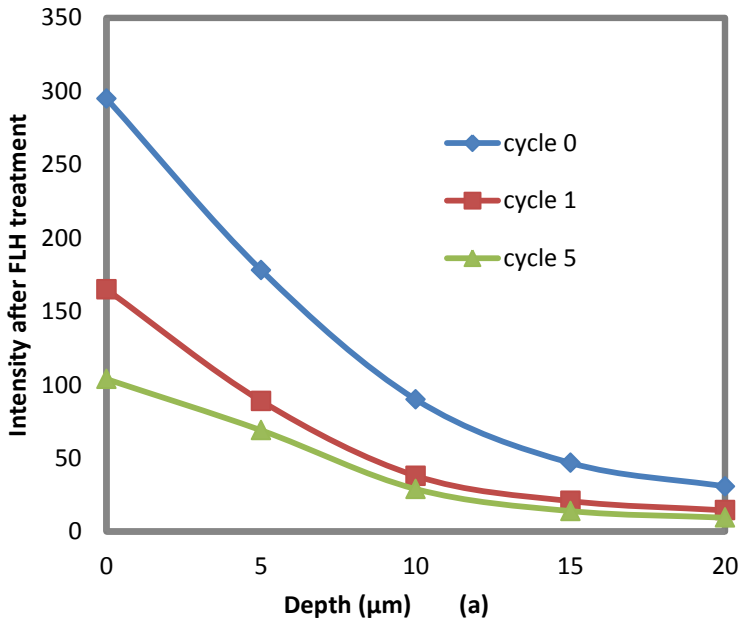

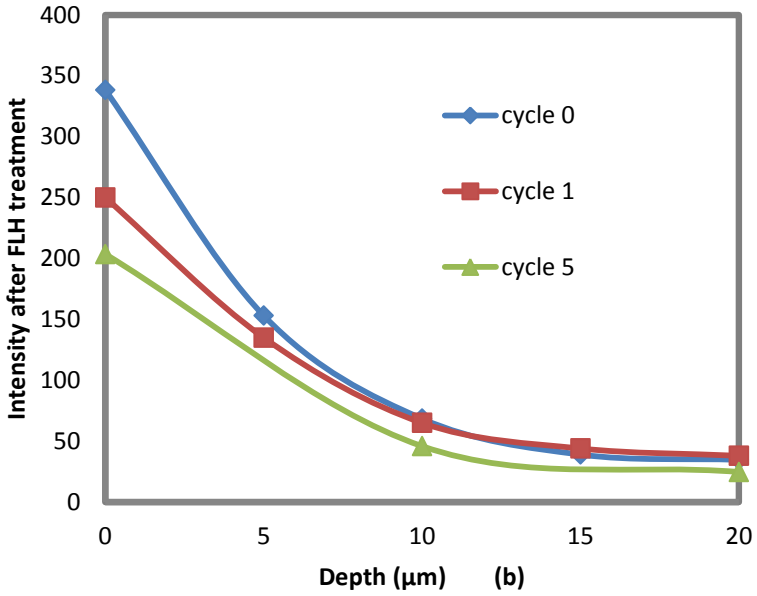

Fig.4.8 (a) Distribution of fluorescence intensity in depth direction for different thermomechanical cycles, probe: pyranine; (b) Distribution of fluorescence intensity in depth direction for different thermomechanical cycles, probe: uranine.

4.3.5 Discussion about result

When the sample is subjected to structural change, the amount of fluorescence dyes immersed in the film becomes smaller, as revealed by Fig. 4.8. It might be attributed to the structural change inside the polymer during thermomechanical cycles. Generally, the reduction of length change ratio is considered as the change in the irrecoverable tensile strain during fabrication or thermomechanical cycles [32]. From the figure, we can detect the change in fluorescence intensity distribution between the sample with large length change ratio and small length change ratio. Therefore, our designed fluorescence spectroscopy has a sufficient sensitivity to determine whether the sample is subjected to relatively large length recovery ratio. While for DSC, there is no difference. At the current state, the experimental condition for immersion of fluorescence dyes and the selection of fluorescence probe is not sufficiently optimized, and a further study is needed. A quantitative correspondence between the length change ratio and the change in fluorescence intensity has not been obtained, we will leave it as a remaining issue.

4.4 Conclusions

(1) SMPU materials used in our experiment have obvious length change ratio difference at thermomechanical cycles at very beginning. After that, length change ratio decreases in a very mild way.

(2) From DSC, SMPU which doesn't undergo thermomechanical cycle is amorphous. After 1, 5, 10 cycles, they have very small amount of crystalline (<1.5%). DSC doesn't show difference from samples after 1, 5, 10 cycles.

(3) The method we developed, based on fluorescence spectroscopy, with the using of LCSM, can detect the internal structural change of the polyurethane (PU) shape memory polymer films, which have different length change ratio. The polymer structural change by thermomechanical cycles was detected by the change in the amount of fluorescence dyes in the film. Experimental results show that our designed fluorescence spectroscopy is sufficiently sensitive to detect the change in fluorescence intensity distribution between the samples with different length change ratio.

References:

1. K. Otsuka and C M. Wayman (eds.), Shape Memory Materials, 1998, New York, Cambridge University Press.

2. H. Tobushi, T. Hayashi, N. Ito, S. Hayashi, E. Yamada, Shape fixity and shape recovery in a film of shape memory polymer of polyurethane series, J. Interll. Mater. Syst. Struct., 1998, 9, 127.

3. A. Lendlein, S. Kelch, Shape-memory polymers, Angew. Chem. Int. Ed., 2002, 41, 2034.

4. JL. Hu, FL. Ji, YW. Wong, Dependency of the shape memory properties of a polyurethane upon thermomechanical cyclic conditions, Polym. Int., 2005, 54, 600.

5. T. Xie, IA, Rousseau, Facile tailoring of thermal transition temperatures of epoxy shape memory polymers, Polymers, 2009, 50, 1852.

6. QH. Meng, J. Hu, A review of shape memory polymer composites and blends, Comp. A., 2009, 40, 1661.

7. QH. Meng, JL. Hu, Y. Zhu, J, Lu, Y. Liu, Morphology, phase separation, thermal and mechanical property differences of shape memory fibres prepared by different spinning methods, Smart Mater. Struct., 2007, 16, 1192.

8. A. Lendlein, R. Langer, Biodegradable, elastic shape-memory polymers for potential biomedical applications, Science, 2002, 96, 1673.

9. HM. Wache, DJ. Tartakowska, A. Hentrich, MH. Wagner, Development of a polymer stent with shape memory effect as a drug delivery system, J. Mater. Sci: Mater Med., 2004, 14, 109.

10. A. Charlesby, Atomic radiation and polymers, 1960, New York, Pergamon Press.

11. JS. Leng, H. Lu, Y. Liu, S. Du, Conductive nanoparticles in electro activated shape memory polymer sensor and actuator, Proceeding of SPIE – the international society for optical engineering. Nanosensors and microsensors for bio-systems, San Diego, CA, United States, 2008, 693109.

12. TE. Grim, JM. Iglesias, KM. Speakes, M. Campos, ST. Pelote, Tractable orthopedic splint or support, US patent, 1999, 6007505.

13. T. Ohki, QQ. Ni, N. Ohsako and M. Iwamoto, Mechanical and shape memory behavior of composites with shape memory polymer, Comp. A., 2004, 35, 1065.

14. B. Lee, B. Chun, Y. Chung, K. Sul and J. Cho, Structure and thermomechanical properties of polyurethane block copolymers with shape memory effect, Macromolecules, 2001, 34, 6431.

15. J. Lin and L. Chen, Study on shape-memory behavior of polyether-based polyurethanes. I. Influence of the hard-segment content, J. Appl. Polym. Sci., 1998, 69, 1563.
16. NS. Claxton, TJ. Fellers, MW. Davidson, Laser scanning confocal microscopy in Encyclopedia of medical devices and instrumentation, 2006, John Willey & Sons Inc.
17. IC. Chang, Acousto-optic devices and applications in Optics II: fundamentals, techniques, and design, 1995, New York, McGraw-Hill.
18. KR. Spring, Detectors for fluorescence microscopy in Methods in cellular imaging, 2001, New York, Oxford University Press.
19. L. Mongan, J. Gormally, A. Hubbard, Calcium Signaling Protocols. 2nd Edition, 2006, Springer.
20. L. Li, S. Sosnowski, C. Chaffey, S. Balke and M. Winnik, Surface morphology of a polymer blend examined by laser confocal fluorescence microscopy, Langmuir, 1994, 10, 8, 2495.
21. L. Sung, J. Jasmin, X. Gu, T. Nguyen and J. Martin, Use of laser scanning confocal microscopy for characterizing changes in film thickness and local surface morphology of UV-exposed polymer coatings, J Coat Technol Res., 2004, 1,4, 267.
22. H. Verhoogt, JV. Dam, AP. Boer, A. Draaijer, PM. Houpt, Confocal laser scanning microscopy: a new method for determination of the morphology of polymer blends, Polymer, 1993, 34, 1325.
23. H. Jinnai, Y. Nishikawa, T. Koga, T. Hashimoto, Direct observation of three-dimensional bicontinuous structure developed via spinodal decomposition, Macromolecules, 1995, 28, 4782.
24. H. Goda and C. Frank, Fluorescence studies of the hybrid composite of segmented-polyurethane and silica, Chem. Mater., 2001, 13, 2783.
25. M. Burke, J. Park, M. Srinivasarao and S. Khan, Diffusion of macromolecules in polymer solutions and gels: a laser scanning confocal microscopy study, Macromolecules, 2000, 33, 7500.
26. E. Pino, A.M. Campos and E. Lissi, Changes in pyranine absorption and emission spectra arising from its complexation to 2,2'-azo-bis(2-amidinopropane), J. Photochem. Photobiol. A, 2003, 155, 63.
27. Q. Li, J. P. Alcantara-Licudine, and L. Li, Determination of phloxine B and uranine in water by capillary zone electrophoresis, J. Chromatogr. Sci., 1997, 35, 573.
28. J. Ying, M. Nishikawa and M. Hojo, Relationship between annealing and shape memory effect of shape memory polyurethane, Adv. Mat. Res., 2014, 936, 140.

29. R. E. Wetton, Effect of orientation on the Tg relaxation of polymers, Eur. Polym. J. 1993, 29, 131.
30. N. Sahoo, Y. Jung, N. Gao, J. Cho, Conducting shape memory polyurethane-polypyrrole composites for an electroactive actuator, Macromol. Mater. Eng., 2005, 290, 1049.
31. B. Wunderlich, Thermal analysis of polymeric materials, 2005, Berlin, Springer.
32. H. Tobushi, K. Okumura, S. Hayashi and N. Ito, Thermomechanical constitutive model of shape memory polymer, Mech. Mater., 2001, 33, 545.

Chapter 5
Conclusions

Neat polymer materials and polymer composites are designed, manufactured, and employed for various purposes. Among these, shape memory polymers (SMPs) are a class of smart materials that has attracted much attention recently. A thorough understanding of SMPs' shape memory properties including tailoring shape recovery ratio is therefore essential, and researchers have been especially interested in finding a more convenient and accurate method of detecting tertiary structural change of SMPs. This thesis focuses on functional polymer – PU SMP's structural change and its assessment. Meanwhile the effect of structural change on mechanical properties in polymer-based composite system with mechanical function was also investigated on a biodegradable carbon fiber (CF) reinforced hydroxyapatite (HA) / polylactide (PLA) composite.

Chapter 2 studies the degradation property of a novel biodegradable CF/HA/PLA composite. This material was designed for bone fixation. CF provides strength, while HA provides bioactivity and PLA meets the requirement of degradation. In a three-month in vitro experiment, we measured shear strength, pH and fracture surface morphology at certain time intervals. We discovered that as the degradation time increased, gaps appeared in the interface between CF and HA/PLA because PLA hydrolyses.. Shear strength remained at the same level, since the carbon fiber did not change much. After 3-month degradation, the pH value of the PBS changed little, since the alkalinity of HA neutralized the acid which degrades from PLA. This provides a reasonable method to design biodegradable bone fixation material.

Chapter 3 is dedicated to studying the relationship between shape memory effect and annealing at a specific temperature for PU SMP from tertiary structural changes point of view. Tertiary structure in polymer is the three-dimensional shaping or folding of the polymer chains. This research is useful to increase shape recovery ratio of SMP with poor recovery behavior and manufacture polymers in complex shape from simple-shape molds. At 65°C, we confirmed that SMPU film's length change ratio due to annealing is actually the same as the change due to

shape memory effect. We also confirmed that we could control shape recovery ratio by controlling annealing time because annealing and shape memory effect have the same mechanism, which is the change of state from low conformational entropy states to the recovery of a stable high entropy state in the polymer.

Chapter 4 develops a method to detect structural changes in PU SMP by measuring the fluorescence intensity of fluorescent dye immersed in this material using laser confocal scanning microscopy. Assuming that the decrease in length change ratio could be attributed to the structural change in the polymer, we compared the fluorescence intensity of immersed fluorescent dyes into the shape memory polyurethane samples with different thermomechanical cycles. Two fluorescent probes (pyranine and uranine) were used. Experiment results indicate a difference in fluorescence intensity distribution between the samples with different length change ratios, which also means that this method is sufficiently sensitive to detect such structural changes.

To sum up, this thesis primarily describes structural changes in PU SMP and results of experimental studies using fluorescence spectroscopy to detect structural changes in SMP. An easy-to-implement approach to tailoring shape recovery ratio by annealing is demonstrated. By using PU shape memory polymer, we have also developed a sensitive experiment method for detecting polymer tertiary structural changes, by fluorescence spectroscopy using laser confocal scanning microscopy, which can potentially be utilized as a non-destructive testing method to defect damage in polymers and polymer composites. In addition, the effect of structural change on mechanical properties in polymer-based composite system was also investigated on CF/HA/PLA biocomposite material.

Although the results presented here have demonstrated the effectiveness of controlling shape recovery ratio by annealing and the approach to detect tertiary structural changes in PU SMP by fluorescence spectroscopy with LCSM, they could be further researched and developed in a number of aspects:

For controlling shape recovery ratio by annealing, we only conducted experiments at 65°C with a recovery time and an annealing time of less than one minute. Results for annealing and shape

recovery at higher temperatures and longer annealing time and recovery time are left for further research. Moreover, in current experiments, a tensile stretch was used as external stimulus to deform SMP to a temporary shape. It is also interesting to conduct experiments with complex temporary shapes.

LCSM is one of the many methods which used to characterize material properties. Measuring fluorescence spectroscopy at different depth of material to obtain structural information is a novel approach. It can be optimized even further by choosing a more suitable fluorescent probe or by changing measurement parameters, etc. Future work will be necessary in order to develop these directions.

List of publications

Journal publications

1. L. Shen, H. Yang, J. Ying, F. Qiao and M. Peng: "Preparation and mechanical properties of carbon fiber reinforced hydroxyapatit/ polylactide biocomposites", J Mater Sci Mater Med. (2009) 20(11): 2259-65
2. J. Ying, M. Nishikawa, and M. Hojo: "Relationship between Annealing and Shape Memory Effect of Shape Memory Polyurethane", Adv Mater Res. (2014) 936: 140-4
3. J. Ying, M. Nishikawa, and M. Hojo: "Fluorescence Spectroscopy to Detect Structural Change in PU Shape Memory Polymer with Different Thermomechanical Cycles", Mater Res Innov. Accepted

Conference publications

1. J. Ying, M. Nishikawa, and M. Hojo: "Effect of Thermal Annealing on the Performance of Shape Recovery of PU film", Manuscript of 2012 Japan Society of Mechanical Engineers Conference (M&M 2012), OS0903, Ehime, Japan. 2012
2. J. Ying, M. Nishikawa, and M. Hojo: "Analysis of Fluorescence Spectroscopy of PU Shape Memory Polymer with Different Thermal Cycles", Manuscript of 9th SPSJ International Polymer Conference (IPC 2012), 12b09, Kobe, Japan. 2012
3. J. Ying, M. Nishikawa, and M. Hojo: "Fluorescence measurement to investigate micro-damage accumulation in plain-woven CFRP composite under fatigue loading", Manuscript of 13th Japan International SAMPE Symposium and Exhibition (JISSE 13), No1403, Nagoya, Japan. 2013

4. J. Ying, M. Nishikawa, and M. Hojo: “Evaluation of micro-damage accumulation in holed plain-woven CFRP composite under fatigue loading ”, Manuscript of 2014 International Society for Optics and Photonics (SPIE), 9063-68, San Diego, USA. 2014